Interactive comment on "Can the boundary
profiles at 26N be used to extract buoyancy-forced
AMOC signals?" by Irene Polo et al.
Anonymous Referee #1

Received and published: 22 April 2020

This paper addresses a significant question and presents interesting results which should be published. There are though some important details that need to be addressed in the presentation of the results before the work can be published. The main result is that, in the model simulations, the variance of density variations on the boundary is, like the AMOC, dominated by the wind on inter annual timescales and only on decadal timescales does the buoyancy forced signal emerge from the "noise" of the wind forced variability. This is not too surprising and the paper could be strengthened by more emphasis on the structure of the variations associated with wind and buoyancy forcing, which has been less studied in previous work. Below are some specific points to consider:

1. More often than not the axes in figures are not labelled and/or units are not given. This is a fundamental requirement.

Response: Thank you for the comment. We have carefully checked the figures and the plots are now correctly labelled with units.

2. In the introduction (l95) it is stated that section 7 "describes the limitations of the interpretations, as well as possible applications e.g. in data assimilation", but there is no mention of assimilation in section 7.

Response: We have removed the sentence from the introduction.

3. Table 1. Its stated that all correlations are significant if greater than 0.3, but doesn't the significance of correlation depend upon number of independent data and hence whether the time series are filtered or not?

Response:

Thank you for this comment. We have calculated the significance with a t-test now with the number degrees of freedom. In table 1 and 2, we have highlighted the significant correlations with a star. The full table of p-values with corresponding effective number degrees of freedom for a two-sided t-test is detailed for the referee below:

p-value and number of effective degrees of freedom Nf / 1yrF	PC1-WB AMOC	PC1-EB AMOC	PC1-EB-PC1-WB	
BUOY	0.63/0.63 10/10	0.75/0.75 7/7	0.67/0.67 9/9	
CTRL	0.2/0.38 103/26	0.20/0.37 241/29	0.25/0.48 64/17	

4. Figure 1b. I would like to see the time series of WIND shown too, without that it is not clear how much variability there is in wind on longer timescales.

Response: We have added the AMOC timeseries for the WIND experiment in new Fig. 2, to compare variability at long timescales, filtered with 1year running mean. The WIND experiments show variability with a peak in 5 years-period in comparison with BUOY and CTRL which has 10 years-period.

5. Figure 1a,b Was the same standardisation applied to each time series? Probably better not to standardise then it would be obvious to the reader what is being compared.

Response: Yes, the timeseries are standardised (for each experiment with respect to their own seasonal standard deviation), in order to compare the variability. Otherwise the comparison could be not fair due to, in part, the different model drifts in each experiment (Megann et al 2014). We have added panels to the Fig. S2 for this clarification. In Fig. S2a it can be appreciated that BUOY experiment has a strongly positive trend compared with CTRL and WIND. Fig. S2b shows the seasonal cycle of the interannual variability. The standard deviation (in Sv) for the 3 experiments is very different; In particularly there is a strong seasonal dependence for CTRL and WIND, but relatively little change through the year for the BUOY experiment. Therefore, we think it is better to compare the normalised anomalies.

6. Notation in the figures is sometimes inconsistent. E.g. "AMOCg" and "1PC" in Figure 1 , but "AMOC" and "PC1" elsewhere. Also abbreviations identifying filtered and unfiltered data vary.

Response: AMOC and PC1 are now consistently used through the manuscript, and in the figures. We also use Nf (for no filtered) and 1yrF (for 1year filtered).

7. Calculation of EOFs (l228) Figure 3c,d show EOFs calculated using data below 800m, so how are these extended up to the surface as seen in the Figures? Some more information is needed in the methods. And are these EOFs for annual or monthly data?

8. The EOFs presented in this paper are dimensional. This is useful, but they are not always calculated this way (sometimes they are normalised) so the text need to make clear what methodology is used here. And it is particularly important to show units on axes to avoid confusion! I presume the variance of the PCs is standardised?

Response: We have better clarified now in the methods Section how PCs are calculated (from line 172). PCs are calculated from monthly density data. The PCs for below 800m (PC-f800) are calculated using only the information from 800m downwards. The PC corresponds to standardised anomalies. However, the EOF pattern is represented as the regression of density anomalies onto the PC-f800. Therefore, the resulting EOFs can have a density signal shallower than 800m. Furthermore, EOFs have density units (density anomalies per 1 standard deviation of the PC).

9. The results of different truncations in Figure 4 suggest anomalies propagate at different speeds at different depths. This would imply that there is no direct correspondence between the EOFs and the modes of boundary waves. This should be discussed.

Response: Thank you for the comment. The correspondence of PCs and boundary wave modes is not direct.

The boundary EOFs are not stationary with time and latitude. Figure 4 shows that the teleconnection between density signals at WB and EB occurs very quickly at 800m-1100m (around 8 months as a fast response) however, at deeper levels for EB, the signal is delayed. There is a possible vertical propagation of the density anomaly at the WB from upper levels (400m) to 2700m.

Different lags in old Fig. 4 could be reflecting different propagation speeds along the equator (Hovmuller diagrams at different depths suggest that the phase speed changes at the equator, not shown here). Whereas the propagation along either the WB or the EB are reasonable to represent similar boundary waves, with coherent combined EOF vertical mode, albeit different modes on WB and EB.

10. Discussion of Figure 8 should highlight how low the variability is in run BUOY over this period.

Response: the AMOC in the BUOY experiment has a peak variability at 10 years (figure 1 in Polo et al., 2014). Similarly, the variability of the zonal density gradient also has a very low frequency in the BUOY experiment (figure 2 in Polo et al 2014). Additionally, it is shown that EB density variability contains higher frequencies in comparison with WB density variability in BUOY (see new Fig. 3c, d).

Considering the short period analysed in Fig. 8 (2004-2009), the BUOY experiment shows a decrease and increase of AMOC at 26N (it is also seen in new Fig. 2 at the end of the period). This trends in AMOC are associated with density variability at WB (red line in new Fig. 3c). Therefore, we agree with the referee about the WB low-frequency density signals in BUOY experiment for long (1958-2009) and short (2004-2009) periods.

However, RAPID shows a decline from 2007 up to 2010, more similar to CTRL and WIND timeseries (new Fig. 9). As a conclusion, RAPID at 2004-2009 period is only representing wind-forced signal. We have tried to make it clear in Section 5 (from line 334).

11. To what extent does the length of the model run affect the results in Figure 9? The run is only about 60 year long so I suspect that for the longer time periods the reduction in the inter-quartile range is a reflection of the length of the model run, rather than the uncertainty of the correlation.

Response: The referee is right. As the period is longer with more years, we have fewer independent periods and therefore less variance in the sample distribution (i.e. the box-plot is smaller). However, the interpretation of old Fig. 9 is still valid. Motivated by old Fig. 8, we realized that for short periods, it was difficult to discriminate buoyancy-forced signals in CTRL (and RAPID). Old Fig. 9 extends this idea using samples of the total model period. Old Fig. 9 (new Fig. 10) suggests that for long periods the correspondence of PC1-WB CTRL and PC1-WB BUOY is straightforward (correlation is high and thus the WB density profile is mainly buoyancy-forced signal).

Other minor comments:

l15 "a propagation speed leading to" is unnecessary

Response: We have removed that part in the sentence.

l16 Abstract - what does maxima refer to?

Response: The sentence has been changed to "The timing of the density anomalies appearing at the eastern and western boundaries at 26N reveals ~2-3 years lags between boundaries at the deeper levels (2600-3000m)". (line 15)

l67 Despite many model studies (insert 'model')

Response: We have inserted the word in the sentence.

Fig 9 "extension of the " is not needed. Often the captions are not as well written as the text.

Response: We have rewritten the caption for figure 9 and also we have checked all the figure captions.

l261 More variance of what?

Response: We have rewritten the sentence to be clearer. The first EOF explains part of the density variance.

l459 What does "simultaneously" refer to?

Response: We have removed the word in the sentence.

l460 "It is worth notice that " Also rephrase to making meaning clear " : : : that, due to : : : , time filtering is : : :"

Response: The sentence has been rephrased as follows: "It is worth noticing that, due to noise from high frequency wind-forcing, time filtering is needed to see a clear signal in GC2."

l470 "but it is not that obvious for the EB" not clear what this is referring to.

Response: The sentence has been rephrased as follows: "… but the propagation up the EB is less clear.".

l476 Which PC1 NEMO (Control, WIND or BUOY? and evaluated over what time period?

Response: "The temporal variability in RAPID WB density modes suggests that wind forcing is still dominating at these short timescales."

l490 1st conclusion - expand what "characteristic signatures " means.

Response: The first conclusion is that we have found density vertical profiles linked to AMOC. Then we explained the characteristics in the following conclusions.

Interactive comment on "Can the boundary
profiles at 26N be used to extract buoyancy-forced
AMOC signals?" by Irene Polo et al.
Anonymous Referee #2
Received and published: 23 April 2020

In manuscript "Can the boundary profiles at 26N be used to extract buoyancy-forced AMOC signals?", Polo et al. examined vertical profile of density in at 26N and its relation to AMOC and to the buoyancy forcing subpolar North Atlantic, in both forced and couple models. Their results suggest that depth structure and the lagged covariances between west and east boundaries at 26N may provide useful information for detecting density anomalies of high latitude origin in more complex model and observations, although time filtering and longer time series are required. The paper is well-organized and well-written over all, but I do have a couple of concerns regarding the realism of the 1 degree model and how fast the density signal transferring from subpolar to subtropical North Atlantic and some clarification and/or discussion are needed.

Title: Spell out AMOC.

Response: The title has been changed.

Line 7: "The temporal variability of the Atlantic meridional overturning circulation (AMOC) is driven : : :"
Response: The sentence has been changed

L135: Given the central relevance to the topic, it is required to include a simple comparison of the T/S/density profiles between model and RAPID for, let's say, a five-year period 2005-2009, to see characteristically how similar/difference they are. And this should be in the paper, not in the supplementary, I understand that profile of density gradient is shown in supplementary, which is fine. Why focus on density gradient there?

Response: As the referee has suggested, we have added the new Fig. 1, which shows the comparison of the temperature, salinity and density profiles at the boundaries between RAPID and CTRL experiments for the period 2005-2009. The figure is commented in the manuscript (from line 138).
Vertical density gradients could be important for the boundary waves phase speed, so we will maintain Fig. S1, which also shows the standard deviation of the density profiles.

L149: Here I think the modeled standard deviation for monthly mean AMOC need to be listed too for comparison with the RAPID value (4.4 Sv).
Response: The standard deviation, after removing the linear trend, using the monthly mean timeseries for NEMO1 is 2.28 and 1.92 Sv for CTRL and BUOY respectively. RAPID reaches double this level (4.4 Sv). This information is now added (from line 153). Additionally, the seasonality of the standard deviation is shown in Fig. S2.

L215: Should Fig. 1a be Fig. 1c?
Response: The reference to Fig. 1a was right. The correlation scores in old Fig. 2c are the correlations between timeseries in old Fig. 2c and timeseries in old Fig. 1a.

L299: The speeds in the forced models are consistent with the lag found between boundaries, but more importantly, are these speeds realistic? It needs some discussions regarding how fast the density signal transfers. A speed of 0.3-0.4 m/s seems really fast to me (until I saw 2m/s later in GC2 experiment), what does this speed represent?
Do we have observational/theoretical supports?

Response: There are works showing the density propagation along western boundary (at deeper levels) from variations of the AMOC (i.e. Kohl, 2005; Hodson and Sutton, 2012; Zhang, 2010). Hodson and Sutton (2012), although they show spatial patterns of the adjustment, they do not specifically give a phase speed of boundary propagation.

However, they showed how the speed of the adjustment is sensitive to model resolution, they found that higher resolution model represents better the propagations at tropical latitudes. Zhang (2010) found different regimes along the latitudinal wave path. From 34N to the equator, she found a propagation coherent with Kelvin wave phase speed.

Johnson and Marshall (2002) have theorised the surface response to an AMOC change through the wave propagation. Other studies have found Kelvin wave propagation from observations and models in the equatorial Atlantic. From linear theory, Atlantic equatorial Kelvin wave speed for first, second and third baroclinic modes are around 2.5, 1.3 and 0.8 m/s respectively (Katz, 1997; França et al., 2003; Illig et al., 2004; Polo et al., 2008). In particular, from sea surface height, Polo et al., (2008) found Kelvin-like waves along the equatorial Atlantic and poleward along the African coast traveling at 1.6m/s, as mixed first and second baroclinic modes.

We had reviewed the adjustment of the AMOC on different model simulation in the introduction section 1, and now we have added more in section 4 (from line 390).

The subpolar density exhibits a significant variability in the last several decades, why we do not see similar variability in the south.

Response: Density over the subpolar gyre is highly variable in comparison with lower latitudes. We assume that part of the energy is lost as it travels southward.

The Labrador Sea is a major source of density variations on the western boundary at depth in many models (Hodson and Sutton, 2012, Polo et al 2014). The propagation in figure hovmuller is quasi-non-dispersive until the equator (around track point 100).

L314 and later in this section: 2004-2010 should be 2004-2009

Response: it is now corrected.

L325: It seems to me an overstatement that the model and observations are very similar here. Not only the PC differ significantly for the first half of the time series, but also the model EOF pattern exhibit much lower magnitude. Also, is the length of the record the only key factor that leads to the difference between BUOY and CTRL (and RAPID)? Although Figure 1b with longer record does show a significant correlation between CTRL and BUOY (in AMOC), the similarity is mainly due to the decadal variability during

1970s-1990s, for which I am not sure if there is any observational support. The similarity/difference between the two experiments display significant time-dependence.

Response: In general, variability in the observations is greater than in the model (see previous comparison of AMOC standard deviations). This is also true in density profiles (see Fig. 1 and Fig. S1 RAPID has more variance at both boundaries at nearly all levels. This is especially important for NEMO1, the low-resolution model does not resolve part of the density variability.

Decadal variability in the AMOC is also supported by the reanalysis products (Wang et al 2010). The similarity of CTRL and BUOY operates at lower frequencies (decadal) not at interannual, which is dominated by the wind (see also Polo et al 2014). This is also true for the comparison we made with RAPID, with only a short record we cannot extract buoyancy-forced signal from the CTRL experiment (new Fig. 9). We have made an effort to explain better this part in the manuscript (from line 332).

L372: The phase speed in GC2 is faster than in the forced simulations by a factor of 5-7 and clearly need some explanations. How robust are the model results, especially, to different model resolution?

Response: There are factors that potentially can influence propagation (and hence the phase speed) of boundary waves in numerical models. i) Model resolution; the along-shore phase speed of a Kelvin wave falls rapidly as grid spacing increases beyond the Rossby radius (Hsieh et al (1983)). Using 2 coupled models, with Arakawa-B grid, Hodson and Sutton (2012) showed that the MOC adjustment proceeds more rapidly in the higher resolution model due the increased speed of western boundary waves. Although in our study, NEMO1 model uses an Arakawa-C grid, it is expected to show difference in higher resolutions versions. ii) Lateral viscosity; increased values of viscosity reduce the along-shore phase speed of coastal Kelvin waves (Davey et al., 1983)). iii) Orientation of the coastal boundary relative to the ocean grid: the along-shore Kelvin wave speed falls as the angle of the coastline to the underlying grid increases (Schwab and Beletsky, 1998). iv) ocean stratification along the path wave.

Additionally, in our study, GC2 is a more complex model since it is a coupled model in comparison with ocean-only NEMO1, which potentially influence the propagation.

Hodson and Sutton (2012) found in coupled model evidence of extratropical atmosphere response and a weak negative feedback on deep density anomalies in the Labrador Sea.

We think that both, resolution and complexity are explaining the differences in the phase speed along boundaries shown in the hovmuller plots (new Figures 7 and 11). However, specific sensitive experiments should be designed and performed in order to properly understand these factors.

This is now discussed more in section 7 (from line 480).

Can the boundary profiles at 26N be used to extract buoyancy-forced ~~AMOC~~Atlantic Meridional Overturning Circulation signals?

Irene Polo[1,2], Jon Robson[1], Keith Haines[1] and Christopher Thomas[1]

[1]Department of Meteorology, University of Reading, Reading, RG6 6BB, United Kingdom
5   [2]Departamento de Física de la Tierra y Astrofísica, Universidad Complutense de Madrid, Madrid, 28040, Spain

Correspondence to: Irene Polo (ipolo@ucm.es)

Abstract. ~~The~~ The temporal variability of the Atlantic Meridional Overturning Circulation (AMOC)~~AMOC circulation~~ is driven both by direct wind stresses and by the buoyancy-driven formation of North Atlantic Deep Water over the Labrador and Nordic Seas. In many models low frequency density variability down the western boundary of the Atlantic basin is linked
10   to changes in the buoyancy forcing over the Atlantic Sub-Polar Gyre (SPG) region, and this is found to explain part of the geostrophic AMOC variability at 26N. In this study, using different experiments with an OGCM, we develop statistical methods to identify characteristic vertical density profiles at 26N at the western and eastern boundaries which relate to the buoyancy-forced AMOC. We show that density anomalies due to anomalous buoyancy forcing over the SPG propagate equatorward along the western Atlantic boundary, through 26N, and then eastward along the equator, and poleward up the
15   eastern Atlantic boundary. The timing of the density anomalies appearing at the eastern and western boundaries at 26N reveals ~~a propagation speed leading to~~ ~2-3 years lags between boundaries ~~with maxima~~ along deeper levels (2600-3000m). Time record required to capture those vertical density profiles in the model is ~26 years. Results suggest that depth structure, and the lagged covariances between the boundaries at 26N, may both provide useful information for detecting density anomalies of high latitude origin in more complex models, and potentially in the observational RAPID array. However, time filtering will
20   be required together with the continuation of the RAPID program in order to extend the time period.

1 Introduction

The Atlantic Meridional Overturning Circulation (AMOC) plays a key role in controlling the Earth's energy budget. It transports warm water to the north, overlaying a return flow southward of colder and denser water (Cunningham et al., 2007). Due to its large net heat transport, low frequency variability in this circulation can have an important impact on Atlantic sea
25   surface temperatures and, therefore, on the wider climate (Knight et al., 2005; Sutton and Dong, 2012). Decadal prediction systems have shown that the upper ocean temperatures over the subpolar gyre can be predicted due to the leading role of the ocean heat transport (Robson et al 2012; Hermanson et al 2014; Robson et al., 2017). In order to make these decadal predictions it is essential that we ensure the best ocean initial conditions are available with a well reproduced AMOC.

30 The RAPID program has been monitoring AMOC and boundary densities at 26N since 2004 (Cunningham et al., 2007; McCarthy et al., 2015). The observational record so far has revealed a large range of AMOC variability on different time-scales; from high frequency (Balan Sarojini et al., 2011), to large anomalies persisting at inter-annual time-scales (Blake et al., 2015; Roberts et al., 2013), or decadal trends (Smeed et al., 2014; Jackson et al 2016). Using different methods, several studies have investigated the observed weakening (since 2005) of the AMOC and have related the trends to earlier high latitude density

35 changes (Jackson et al, 2016; Robson et al 2014, 2016).

The AMOC circulation is driven both by direct wind stresses and by the buoyancy-driven formation of North Atlantic Deep Water (NADW) over the Labrador and Nordic Seas. Theories of the response of the AMOC and the ocean gyres to wind stress or buoyancy input rely on energy being transmitted through the ocean by planetary Rossby waves, or along the ocean margins

40 by boundary waves (Johnson and Marshall, 2002; Hirschi et al., 2007; Hodson and Sutton, 2012; Jackson et al., 2016). In particular, changes in the NADW may produce a chain of events in the North Atlantic on a range of time-scales from months to decades. The adjustment has been studied in an extensive literature. Some model studies (Kawase, 1987; Huang et al., 2000; Johnson and Marshall, 2002; Getzlaff et al 2005; Marshall and Johnson, 2013) suggest that AMOC anomalies propagate with boundary Kelvin wave speeds resulting in a very short lead time (of order a few months) between subpolar and subtropical

45 AMOC changes. Roussenov et al (2008) suggested that this boundary propagation may also involve higher mode Kelvin and topographic Rossby waves, leading to longer propagation times (of order years). The advection of the NADW outflow also moves down the western boundary more slowly in the Deep Western Boundary Current (DWBC), although lagrangian float observations show that a large fraction of this NADW moves away from the boundary and enters the ocean interior near the Flemish Cap and the Grand Banks (Bower et al., 2009). Using a coupled climate model Zhang (2010) and Zhang et al. (2011)

50 showed AMOC variations associated with NADW formation propagating more in line with the advection speed, with much longer lead times (several years) between subpolar and subtropical AMOC variations. Getzlaff et al. (2005) have shown that the high latitude adjustment to AMOC anomalies can result from a superposition of a fast wave response and a slower advective signal in ocean model experiments with different resolutions. Interestingly, the speed of propagation along boundaries of the density/velocity anomalies related to AMOC changes is found to be model-resolution dependent (Getzlaff et al 2005; Hodson

55 and Sutton, 2012). These propagating density anomalies will also affect the geostrophic AMOC variability at 26N.

Model simulations clearly show a large range of mechanisms leading to AMOC variability at latitude 26N (Hirschi et al., 2007; Biastoch et al., 2008; Cabanes et al., 2008; Duchez et al., 2011; Polo et al., 2014; Pillar et al., 2016). Buoyancy forcing generally operates from inter-annual to decadal time-scales, while the wind forcing mostly acts from intra-seasonal to inter-annual time-

60 scales (Cabanes, et al., 2008; Kanzow et al., 2010; Duchez et al., 2011; Polo et al., 2014; Pillar et al., 2016). Using an adjoint OGCM, Pillar et al (2016) have found that inter-annual to inter-decadal AMOC variability of ~5 Sv amplitude can be excited by heat fluxes in the subpolar North Atlantic, with freshwater fluxes playing a more minor role. Due to the adjustment from higher latitudes, Western Boundary (WB) density anomalies explain most of the variance in the zonal density gradients, and

hence geostrophic transports, at 26N, especially at decadal time-scales (Hirst et al., 2007; Polo et al., 2014). The Eastern Boundary (EB) explains only a small part of the inter-annual variability in zonal density gradients in the upper 1500m, and this is mostly due to local wind forcing (Polo et al., 2014).

Despite the many model studies showing boundary wave connections between the Labrador Sea and lower latitudes, and their importance for the AMOC, less work has been done on the vertical structure of these anomalies, and yet it is the vertical density structure at 26N that is primarily measured by the RAPID array. We now benefit from more than 10 years of boundary density records at 26N, and therefore can consider how best to use the vertical structure in these data to study the lower frequency variability. If low frequency signals can be identified from the vertical structure this would help us to assimilate the most important signals that need to be reproduced in climate forecast models. This poses the question we address in this paper; *can we extract the buoyancy forced signals from vertical density profiles, such as those sampled at 26N?*

An earlier attempt to extract buoyancy signals at 26N was made by Polo et al (2014, hereafter PA14) using a NEMO 1° OGCM forced with full ECMWF reanalysis meteorology from 1958-2010, denoted as the CTRL experiment. This CTRL experiment was compared to runs using only inter-annual wind or buoyancy forcing, allowing separation of buoyancy from wind forced variations in the AMOC. PA14 found that the buoyancy-forced AMOC anomalies at 26N could be related to changes in deep water formation over the Labrador Sea some years before. Although they showed a coherent WB vertical signal at 26N, they were not successful in isolating the buoyancy forced signal in the CTRL experiment, due to the confounding influence of the wind forced variability. They did not look in detail at the propagation or how the vertical structure associated with the buoyancy forced anomalies develops. In the present work we extend the work of PA14 by (i) developing statistical means of isolating the buoyancy forced AMOC variability from the full variability in the CTRL using the density profiles at 26N; (ii) analysing the propagation of the buoyancy forced signals from the Labrador Sea down to the subtropics; and (iii) developing statistical covariance relationships linking the AMOC to the Labrador Sea that might potentially be used in a data assimilation context to modify the low frequency AMOC variability. The diagnostics developed are also tested on RAPID observations and on output from the state-of-the-art coupled model HadGEM3-GC2 (Williams et al 2015), which has a ¼° NEMO global ocean.

In this paper Section 2 presents the methodology used to analyse AMOC variability and its sources in several runs of the NEMO model (1°x1° horizontal resolution) driven by different components of ECMWF atmospheric forcing from 1960-2012, as in PA14, but now including some validation of the boundary density variability in the CTRL run against the RAPID observations. Sections 3 and 4 describe the modes of the 26N density profile variability in the model and the associated propagation occurring upstream and downstream, respectively. Section 5 describes a statistical analysis of boundary densities in the RAPID observations and compares these modes with the NEMO experiments. Section 6 discusses density variability in

the coupled experiments GC2, Section 7 describes the limitations of the interpretations~~, as well as possible applications e.g. in data assimilation.~~. Finally, Section 8 summarizes the main conclusions.

2 Methodology

This section describes the model experiments and statistical methods used to understand the boundary density variability and
100   its relation to the AMOC variability.

2.1 Forced experiments

The forced ocean-only model (hereafter NEMO1) is based on NEMO V3.0; it uses the tripolar ORCA grid in a global configuration with 1°x1° horizontal resolution and a tropical meridional refinement to 1/3°. The model has 42 vertical levels with thicknesses ranging from 10m at the surface to 250m at the ocean bottom. Initial conditions are taken from the second
105   iteration of a 50-yr cyclic model spin up, each cycle spanning the period 1958–2009 (Balmaseda et al., 2013). The model is forced with daily atmospheric fluxes as boundary conditions taken from the ECMWF Re-Analysis ERA-40; (Uppala et al. 2005) from 1958 to 1978, and the Interim ECMWF Re-Analysis (ERA-Interim; Dee et al. 2011) from 1979 to 2009.

The control experiment (CTRL) is forced with time-varying daily surface heat, freshwater and momentum fluxes for the period
110   1958–2009. The sea surface temperature (SST) is weakly relaxed to daily values with a relaxation time scale of ~1 month, while the sea surface salinity (SSS) is restored to climatological SSS with a time scale of 1 year. There is no ice model; instead, wherever the sea ice concentration in the observations exceeds 55%, the model SSTs are nudged more strongly (1-day time scale) to the freezing point (-1.88ºC). The restoration to SSS and SST is stronger under sea ice (30 days and 1 day, respectively).

115   Following the work of PA14 we also have a set of simulations where the momentum and buoyancy forcing is decoupled from one-another. In the experiment referred to as BUOY, the momentum flux is taken from the ERA-Interim 1989–2009 seasonal climatology, while the buoyancy forcing (heat, freshwater flux, and SST) is still inter-annually varying. In the experiment referred to as WIND, the momentum flux is fully varying, but the buoyancy forcing is from the same seasonal climatology. These experiments allow us to identify and distinguish the AMOC signals and processes associated with buoyancy and wind
120   forcing, to the extent that they are independent. We use the BUOY experiment as reference for the buoyancy-forced only signals, and the CTRL experiment as the "truth" which includes both buoyancy and wind forcings, as well as the interaction between them. Where appropriate, we also include the WIND experiment and SUM (as the sum of anomalies from BUOY and WIND). Results are discussed in Sections 3, 4.

2.2 Coupled experiment

We also analyse 120 years of monthly-mean data from a control run of the high-resolution coupled ocean-atmosphere model HadGEM3-GC2 (hereafter GC2, Williams et al 2015). The ocean component is NEMO v3.4 with the ORCA025 tripolar grid configuration, using Met Office parameters for "Global Ocean 5.0" (GO5.0, Megann et al 2014), with the CICE sea-ice model. The atmosphere component is GA 6.0 of the Met Office Unified Model (UM; Walters et al 2011) at a resolution of N216 (~60Km in mid-latitudes) and 85 levels. This model was used in the Met Office seasonal and decadal prediction systems (GloSea5 and DePreSys3 respectively). The model has been used to study the North Atlantic variability and its predictability (Menary et al 2015; Williams et al 2015; Ortega et al 2017; Robson et al., 2016). Results are shown in Section 6.

2.3 Model evaluation

We use the RAPID array (McCarthy et al., 2015; Smeed et al 2017) to evaluate the boundary densities in the model. We use the merged profiles at the Western Boundary (26.52N, 76.74W) and Eastern Boundary (26.99N, 16.23W) for the period April 2004 to December 2009.

Figure 1 shows the profiles of temperature, salinity and density at the boundaries for RAPID and CTRL experiment. The main differences occur at the EB in the upper 1000m, especially in temperature and salinity (Fig. 1a, b), probably due to a bias in the location of the Mediterranean waters. Beneath 2000m, the variables in CTRL and RAPID are very similar.

NEMO1 and GC2 are both able to capture important aspects of the observed boundary density profiles such as the mean vertical density gradients (N^2, Fig. S1a). On the WB the profiles are similar between 1500m to 4500m but the model stratification is stronger between 300-700m. The EB profiles are similar at all levels below 500m (Fig. S1a). However, the NEMO1 model underestimates the density variance at all levels, especially at the WB, while GC2 has a more realistic variance on the WB at depth (Fig. S1b).

The AMOC at 26N in NEMO1 has a time mean (12Sv) and maximum (18 Sv) at a depth of 1000m in the CTRL experiment. The mean AMOC is higher in the BUOY experiment by ~2 Sv. The AMOC measured at 1000m has a prominent trend in the BUOY experiment (+3.2 Sv in 52 years), but the trend is not significant for the CTRL (-0.2 Sv in 52 years). The AMOC seasonal cycle (not shown) in the CTRL presents a maximum in boreal winter with a secondary peak in boreal summer, which is also reproduced in the BUOY experiment. The annual cycle defined as the difference between the maximum (in boreal winter) and the minimum (in boreal spring) is 3.9 and 4.9 Sv for the CTRL and BUOY experiments. After removing the linear trend and the seasonal cycle the standard deviation of both experiments is similar: 2.28 and 1.89 and 1.4392 Sv for CTRL and BUOY respectively (see also Fig. S2 for the AMOC distributions). The AMOC at 26N in the RAPID observations presents a mean and maximum of 17 and 31 Sv respectively from 2004-2014, with monthly standard deviation of 4.35 Sv., which double

the standard deviation for the CTRL experiment. Trends have been reported for RAPID data of -0.6Sv/year (Smeed et al 2014; 2018) which could be part of a longer variation cycle (Smeed et al 2018, Jackson et al 2016). Results from the modes of variability at the western boundary density profile are shown in section 5.

160 **2.4 Statistical analysis**

Model experiments are first sampled at the western and eastern Atlantic boundaries at 26N to simulate the monthly-mean density profiles from the RAPID array. Empirical Orthogonal Function (EOF) analysis of these density profiles is used to obtain vertical modes of density variability and related timeseries of Principal Components (PCs) which together represent the largest fractions of the total variance (Bretherton et al., 1992).

165

Before calculating the EOFs, the data are processed to remove the seasonal cycle and linear trends. Unlike in PA14, density anomalies are weighted by the thickness of each layer to ensure that all points are appropriately represented for the total density variability. The EOF analysis is computed for the individual boundaries; Western Boundary (WB) and Eastern Boundary (EB), and also for the combined anomalies at both boundaries. Finally, we have explored the combined EOFs by time lagging the 170 eastern boundary variability in order to understand related signals from both boundaries.

The PC timeseries is normalised (the units are standardised anomalies) and the associated EOF is represented as the regression map of the density anomalies (in kg/m3) on to the PC timeseries. Therefore, the EOF pattern has density units (density anomalies by 1 standard deviation of the PC). The PC is calculated from monthly data of the density profiles. The PC from 175 800m (referred to as PC-f800) is calculated using only the information from 800m downwards. However, the resulting EOF pattern, by computing regression map, can have a density signal shallower than 800m.

Regression analysis of the PC time series ~~associated with these EOFs on~~ on other fields (e.g. 3D density) allows us to detect spatial patterns and depth structures of the propagating modes associated with the EOFs at 26N. We show regression and the 180 correlation coefficients where they are statistically significant at the 95% confidence level, according to a Student's t-test for the effective number of degrees of freedom (Metz, 1991).

2.5 Spectral analysis

In order to remove the high frequencies in the timeseries in section 3, we have used a one-year running mean filter. This filtered timeseries is obtained by taking the average of a data subset (13 months) which is centered in a monthly time step (von 185 Storch and Zwiers, 1999).

Spectral analysis is used to decompose timeseries to show signals that lie within different frequency bands. The analysis is performed in order to identify the frequencies involved in the propagation of density anomalies at different depths. Power

6

spectra of the time series are obtained using the multi-taper method, which provides more degrees of freedom and therefore

190 more significance (Thomson 1982). The power spectra are tested against the hypothesis that the signals are generated by a first-order autoregressive process AR(1) with the same time-scale as the original, yielding a red noise spectrum, and the 95% confidence limit for the rejection of red noise hypothesis is applied. Additionally, when we have a large internal variability, we use the decomposition in order to filter some of the timeseries using a Lanczos (1956) filter. This is done in particular for the control GC2 run simulation.

195

We have used the Radon Transform (RT) function (Dean 1983) in order to estimate the phase speed of propagation of density anomalies. The angle of the maximum RT standard deviation determines the propagation phase speed. We calculate the RT every 0.1 degrees. The phase speed averaged for the Hovmöller diagrams has been estimated at 3000m level for CTRL and BUOY experiments.

200 **3 Modes of vertical density variability at the 26N boundaries**

3.1 Linearity of AMOC and the boundary density signals in the NEMO1 model

The forced ocean model experiments enable us to isolate the boundary density variability associated with buoyancy forcing i.e. from the BUOY experiment, as noted by PA14. We focus here on developing the vertical density fingerprint of this signal and using it to identify the buoyancy forced AMOC signal as it appears in the CTRL run.

205

Figure ~~1a~~2a shows the monthly AMOC (defined as total AMOC minus Ekman component) variability, defined as the integral of the meridional transport at 26N down to 1028m, for both the CTRL and BUOY experiments (as in Fig. 1a in PA14). There is a prominent decadal signal in both CTRL and BUOY with peaks in 1975, 1985 and 1995, although CTRL also shows additional monthly and inter-annual variability. The decadal signal of the AMOC timeseries has also been reproduced by

210 reanalysis products (Wang et al 2010; Karspeck et al., 2015). The monthly-mean timeseries correlate at 0.43, but the correlation rises to 0.62 when using a 1 year running mean filter (Fig. ~~1b~~2b). Wind forced inter-annual variability explains most of the remaining differences; when the 1-year smoothed AMOC anomalies from BUOY and WIND are summed the correlation with CTRL rises to 0.86 (SUM in Fig ~~1b~~2b).

215 ~~The majority~~Most of the boundary density variability is also recreated in BUOY and WIND. The correlations between boundary density anomalies in the CTRL and SUM are shown as a function of depth in Fig. ~~1c~~2c-d. For the WB, most of the variability is linearly reproduced by SUM from 1800m to 4000m (Fig. ~~1c~~2c and Fig. S3). For the EB SUM explains most of the variability seen in the CTRL experiment at all depths (Fig. ~~1d~~2d and Fig. S3). A 1yr low pass filtering does not influence the correlations for the WB, although for the EB filtering reduces the correlation at some depths. We now relate this density

220 variability with the AMOC signals in Fig ~~1a~~2a, b.

7

3.2 EOFs of boundary density profiles

Figure 2̶3 shows the Principal Component time series of the first EOF computed using monthly density profiles on the western and eastern boundary at 26N for the CTRL (blue) and BUOY (red) experiments. As density profiles near the surface contain significant noise, we calculate the PCs for both full depth profiles (f0m, Fig. 2̶a̶3a-b) and only from 800m downwards (f800m, Fig. 2̶c̶3c-d). The full depth PCs in Fig. 2̶a̶3a both show substantial high frequency noise, and the CTRL timeseries does not correlate well with AMOC variability from Fig 1̶a̶2a. However, when only retaining densities below 800m, in Fig. 2̶c̶3c, the BUOY and CTRL PCs closely match each other (r=0.80) and both now correlate with the AMOC time series in Fig. 1̶a̶2a (r=0.33 and r=0.88 for the CTRL and BUOY respectively). These f800m EOFs also explain more of the deeper density variance. Note that, adding a 1-yr filter to the PC-CTRL timeseries increases the correlations with the CTRL AMOC variability to 0.47 (Fig. 2̶c̶3c). However, for the BUOY experiment the temporal filter has little impact on the correlation between PC and AMOC timeseries (0.89).

Figures 2̶b̶3b and d show the corresponding eastern boundary density EOF timeseries for full depth and below 800m variability. The full depth PC is rather different to that on the western boundary, and also to the AMOC variability itself. However, when only the deep variability is retained, the inter-annual variability in BUOY is more similar to the western boundary buoyancy driven variability. In CTRL there is still considerable high frequency wind generated variability, however, when a 1-yr filter is introduced the buoyancy forced AMOC related signal also becomes visible on the eastern boundary, and the correlation with the AMOC rises to 0.42 (Fig. 2̶d̶3d). All correlations are summarised in Table 1.

In order to understand the gain of truncating the density profiles in the EOFs and theirs limits, Fig. 3̶a̶4a-b summarises correlations between leading PCs at the boundaries and AMOC timeseries in the CTRL experiment by increasing the truncation level for the density profiles. For the WB, maximum correlation is found simultaneously at all truncations especially for deeper levels (Fig. 3̶a̶4a). In contrast for the EB simultaneous correlations are always low even with a 1 year filter but correlations increase greatly when a lag to the AMOC is applied (Fig. 3̶b̶4b). Correlations still require a 1 year filter to remove noise but now peak at 0.7 with a lag around 2-3 years, with the deeper signals also showing the longer lags. Similar lag increases of EB correlation is seen for the BUOY experiment (not shown). The nature of this lag in the EB-AMOC correlation is related to the link between boundaries and it will be discussed along in the next section.

Figure 3̶c̶4c-d shows the vertical structure of density anomalies associated with the leading EOF modes for both boundaries using the 800m depth truncation and monthly-mean data for the three experiments CTRL, BUOY and WIND. The leading EOFs are very similar between CTRL and BUOY on the WB, with maxima between 1200m and 4000m. Note that in PA14 Fig. 3b, their PC-WB in the CTRL experiment with only 500m depth truncation was substantially different and was mainly wind-driven. The WIND experiment has much less variability at greater depths and the PC is uncorrelated with the PC-WB

8

from CTRL (r=0.09, Fig. ~~3c~~4c). Therefore, on the WB, Fig.~~s 2c~~ 3c and ~~3c~~4c show that the EOF analysis successfully extracts the buoyancy-forced signal related to the AMOC in the CTRL.

On the EB the leading EOFs, even below 800m, show more correspondence between CTRL and WIND (Fig. ~~3d~~4d, with PC correlations r=0.87). This explains why further filtering and the application of a lag to the PC timeseries in Fig ~~2d, 3b~~. 3d, 4b is needed to extract the weaker buoyancy-forced AMOC-related signal on the EB. The relationship between these buoyancy driven density variations at both boundaries is now explored further.

3.3 Relationship between boundaries

Figure ~~4a~~5a shows lead-lagged correlations between the WB leading PCs (computed from 800m depth) and the EB at different depth truncations in the CTRL experiment. Dashed (solid) lines indicate PCs without (with) the application of 1year running mean filtering. For truncations deeper than 1600m the highest correlation is found when EB is lagged, up to 30 months (Fig. ~~4a~~5a), revealing longer links between boundaries for deeper levels. However this lag is much less clear when shallower depth are retained and substantial WB-EB density correlations can still be seen with lag0, unlike in Fig ~~3b~~. 4b. Even in the BUOY experiment only when the EB EOFs are truncated to below 1600m is a strong lag clearly seen between the boundaries, again reaching up to 30 months for the deepest signals (Fig. ~~4b~~5b).

In order to reduce upper level noise at the EB and to bring out the deep density signal connecting the boundaries more clearly we compute the combined EOF while truncating the EB to below 1600m, which shows a maximum in the WB-EB correlations for CTRL (Fig. ~~4a~~5a). The new combined EOF shows similar WB structure for all lags (Fig. ~~4c~~5c) with a deeper signal around 2000m on the EB (Fig. ~~4d~~5d). Figure ~~4e~~5e shows the timeseries, which is very similar to the PC1-WB in Fig. ~~2c~~3c. The new combined EOF explains more density variance in CTRL (43% compared to 40~~%)~~% explained by PC1-WB) and a slightly longer lag between WB and EB (18 months in CTRL and 25 months in BUOY, not shown).

We conclude that the deep densities on the EB contain a very clear signal of the buoyancy forced AMOC variability but that this signal plays no detectable role in the direct (lag 0) control of the AMOC. The EB lag can also be seen in relation to PC-WB density although the signal is less clearly lagged, probably reflecting the noise still present in the upper layer densities on the WB.

The WB clearly contains the core density information on the buoyancy-forced AMOC changes at low frequencies. Using PC1-WB, we will now identify the propagating density signal connecting the boundaries (section 4) and search for similar signals in RAPID data (section 5), and in the higher resolution GC2 model (section 6).

4 Propagation of the buoyancy-driven signals

Motivated by the lagged signal at the EB, we analyse the i) spatial coherence of the anomalies at deeper levels (~3000m), and ii) the propagation fingerprints of the connecting signals.

4.1 Spatial regression patterns

Figure ~~5~~6 shows the spatial density anomalies averaged 2700-3000m, regressed onto the PC1-WB for the CTRL and BUOY experiments respectively, at different lags. At these deep levels the regression patterns in CTRL (Fig. ~~5a~~6a-c) and BUOY (Fig. ~~5d~~6d-f) are very similar to each other. This agreement suggests that, although the magnitude of the regressions are stronger in BUOY, we are identifying the same signal in both experiments. The density signal in the Labrador Sea appears from lag -30 (Fig. ~~5a~~6a, d) and intensifies and propagates down the WB to the Equator (Fig. ~~5b~~6b, e), and then across the equator and poleward at the EB (Fig. ~~5c~~6c,f).

Density regressions at shallower levels (900-1300m) against PC1-WB in the CTRL experiment (suggested by the maximum in the EOF profiles in Fig. ~~3~~4) also finds anomalies beginning near the Labrador Sea, leading PC1-WB by 30 months, and a pattern of equatorial Kelvin and Rossby-waves as in Johnson and Marshall (2002) from lag -30 to lag ~0 (Fig. S5). However, the absence of such tropical signals in BUOY at long lags (lag -30) shows that these could be wind driven Ekman pumping signals (see supplementary material in Fig. S6). Therefore, we concentrate on the deeper signal which is clearly related to buoyancy.

4.2 Wave path and phase speed

Figure ~~6a~~7a shows the wave-track defined following the signals in Fig. ~~5~~6 and using the topography at the 3269 m model level. The wave-track starts in the Labrador Sea (60N) and proceeds southwards to the equator. We plot it along the equator and then North along the eastern boundary to 55N. The path avoids entering into the Gulf of Mexico but at these depths this is not expected.

The Hovmöller diagram along this path (Fig. ~~6b~~7b) shows the propagation related to peaks in the deep water formation at high latitudes for the CTRL experiment (BUOY is very similar, not shown). Density anomalies propagate continuously along the track from the Labrador Sea around to the British Isles. The propagation shows density maxima in 1975, 1985 and 1995, also seen as peak-AMOC years in Fig.~~s~~ 1-2. Additionally, the propagation speed from the Radon transform is similar for both experiments (0.41 and 0.31m/s for the BUOY and CTRL respectively). This phase speed is consistent with the lags found between boundaries (i.e. density anomalies in CTRL will take ~25 months to travel between WB and EB following the defined track). Background currents at 2700-3000m level for the CTRL is shown in supplementary material (Fig. S4).

Figure 78 shows the regression of density anomalies from Fig. 6b7b onto PC1-WB for the CTRL and BUOY experiments. The density anomalies in both experiments show a continuously propagating pattern from the Labrador Sea right around to 40N on the eastern boundary. The signal is stronger in BUOY, as noted in Fig. 56, but otherwise the regression patterns are very similar.

320

Importantly these propagating buoyancy-related signals are clearly seen in the CTRL experiment where wind and buoyancy forcing are both applied, again suggesting that the analysis is extracting the same buoyancy forced processes. Therefore, the diagnostic methods developed should allow identification of similar signals in other models and in the observations. In the next section we look for similar buoyancy-forced signals in the RAPID observations.

325 5 Modes of WB density variability in RAPID data

The RAPID timeseries dataset is considerably shorter than the datasets analysed for buoyancy signals in the NEMO model. Nevertheless Fig. 89 uses the same EOF analysis on the WB density profile for the RAPID array and for the NEMO experiments for the common period 2004-20102009. The first two leading EOFs and their PCs indicate inter-annual variability in RAPID data (black lines in Fig. 8a9a, c). EOF1 has a maximum density anomaly at ~1000m (with a maximum of 0.04 kg/m3 in Fig. 8b9b), while the second mode describes variations at deeper levels (~3000m, Fig. 8d9d).

330

The density EOFs of the WB in both the CTRL (blue lines) and WIND (green lines) experiments for the common period 2004-20102009 look quite similar to the EOFs from the RAPID array, in particular with EOF1 peaking at around 1000m and EOF2 peaking much deeper at ~3000m (Fig. 8b9b, d). However, the density anomalies in RAPID modes are larger than in model modes (larger amplitude of density variance in RAPID compared with CTRL is also seen at all depths in Fig. S1).

335

However in BUOY (Fig. 9, red lines) the absence of inter-annual wind variability means that the deep 3000m peak shows up as EOF1, associated with a decrease up to 2008 and an increase after up to 2010 (Fig. 9a, similar to the signal at the end of the period in Fig. 3c). which is more comparable to EOF2 from RAPID, while BUOY EOF2 shows very little clear density signal at depth, associated with a more interannual variability (Fig. 9c-d).

340

The PC1 time seriestimeseries in CTRL and WIND also look very similar to PC1 from RAPID, reaching a peak in 2007 and declining to 2010 (Fig. 8a9a). For these common 6 years of simulation 2004-20102009, the wind-forced inter-annual density variability on the WB is remarkably well captured by the model.

345

Figure 910 shows the statistics of the correlation between the leading WB mode for CTRL and both, WIND (Fig. 9a10a) and BUOY (Fig. 9b10b) experiments using different numbers of years for each sub-period (x-axis). Figure 9a10a (first box) shows

11

the test of sampling 6 years periods (as we have in 6 years in the common period in Fig. 8a9a). For all 6 year periods selected

between 1958 and 20102009 we also found that EOF1 and PC1 in CTRL and WIND agreed well (Fig. 9a10a, first box), even

350   in periods when the buoyancy signal was known to be changing rapidly. This dominance of the wind forcing over short time

periods is not surprising and was noted previously (PA14).

We find that typically 16 years of data are needed to find a significant (above 0.35) correlation between CTRL and BUOY

(Fig. 9b10b), however the leading mode in CTRL may still be a mix of wind and buoyancy forcing (as seen from Fig. 9a10a).

355   The best extraction of buoyancy forcing signals occurs when we have periods longer than 35 years, when the wind-forced

signal nearly disappears (Fig. 9a10a). Figure 9c10c shows the correlation between the PC1-WB and the AMOC timeseries for

the CTRL and different periods. This would represent how much variance of AMOC can be explained by the PC1-WB. For

periods with more than 25 years, PC1-WB in CTRL experiment is able to explain more than 25% of the AMOC variance

(r>0.5), therefore, it is still able to extract an AMOC-related signal at 26N (Fig. 9c10c).

360

Although EOF2 from CTRL and RAPID both represent deeper density variability (Fig. 8d9d) they are still dominated by wind

forcing over this short time period, and we note that EOF2 from WIND shows the same deep density peak. The PC2s from

CTRL and WIND show very similar time series and even the RAPID PC2 shows a considerable level of agreement with CTRL

and WIND (Fig. 8c9c). However PC1 from BUOY, which has a similar EOF but represents only the buoyancy forced

365   component, has only lower-frequency changes with no relationship to the other timeseries (Fig. 8a9a). The BUOY PC2

timeseries (Fig. 8c9c) also shows no comparable variability.

Therefore, the short record of the RAPID array would not allow us to follow buoyancy-forced signal from the NEMO1 model.

Hence, it appears likely that the variability seen here in the RAPID record, both at shallow and deeper depths, is mainly related

370   to wind-forcing (both PC1 and PC2 in CTRL experiment and RAPID show agreement in Fig. 89). Note that the same EOF

analysis using the longer record now available for RAPID data (2004-2018), but not for these model results, still gives similar

density profiles to Fig. 89 (not shown).

The NEMO1 model results suggest that the lower frequency buoyancy forced signals from higher latitudes may start to

375   dominate over the wind forced signals after ~25 years of RAPID data have been collected, when their leading density variability

should show up at deeper depths ~3000m. In the next section we look at the ability of the analysis to extract buoyancy forced

signals and their propagation in higher resolution HadGEM3-GC2 coupled model run, which is the current UK operational

coupled model.

6 Boundary density in a high resolution coupled model

6.1 Density propagation in GC2

380

Figure ~~10a~~11a shows a wave track for the GC2 model (section 2.2) bathymetry using the 3138m level boundary, and figure ~~10b~~11b shows the Hovmöller diagram of the density anomalies for 120 years along this track , after applying a 2 year low pass filter as GC2 is much noisier at higher frequencies (see methods). We notice that the high frequency density anomalies (<2years period) in a similar Hovmöller are not presenting propagating signals but very noisy signals (not shown), therefore we suggest

385 that the high frequency signal is dominated by local Ekman pumping.

Anomalies propagate down the WB from ~40N (track point 200) to the equator and across to the EB. These signals can be traced back across the Gulf Stream to subpolar latitudes (points 100-200), but only appear as lower frequency decadal variations in the subpolar gyre and into the Labrador Sea (points 0-100). The Radon Transform phase speed is ~2m/s, which

390 is faster than the phase speed calculated in NEMO1 at the same depth (Fig. ~~6~~7), and closer to the theoretical and observed Kelvin wave propagation speed- (Illig et al 2004; Polo et al 2008). Other authors, using models of different complexity, have found a similar phase speed of density anomalies from AMOC variations propagating along the western boundary (Getzlaff et al 2005; Zhang, 2010; Marshall and Johnson, 2013). Therefore, as the density anomalies propagate down the deep western boundary, we would expect to find this deep density variability signal using the EOF analysis.

395

6.2 EOFs at the WB in GC2

Figure ~~11a~~12a shows the vertical density profiles associated with the first two EOFs from 800m downwards at the 26N WB in the GC2 experiment. The profile location is the closest grid-point to the western wall at the Bahamas, which reaches the bottom at 3200m, and the first 2 EOFs explain more than 70% of the total variance. The EOF1 shows an equivalent barotropic

400 vertical structure peaking near the bottom ~3000m (blue line) while EOF2 changes sign between 900m and 3000m (red line).

The PC1 timeseries associated with EOF1 is plotted in Fig. ~~11b~~12b (blue line). Unlike in NEMO1 this PC1 shows high frequency variability which is nevertheless still correlated with the AMOC-Ekman (i.e. the peak AMOC stream function at 900m after the variability due to Ekman has been removed) without filtering at r=0.45, rising to r=0.49 with high-pass (<2

405 years) filtering. However, PC1 becomes less correlated with the AMOC after 2 year low-pass filtering, r=0.25 (Table 2). In contrast, for PC2 the unfiltered correlation with the AMOC-Ekman is low (r=0.13) but this increases with 2 years low pass filtering (r=0.32, Fig. ~~11c~~12c, Table 2). As density anomalies at deep levels are able to be excited by wind alone (already seen in both NEMO1 and the RAPID observations in Fig. ~~8~~9), the two EOFs in GC2 both capture some wind and buoyancy forcing, with variability signals in both PC1 and PC2.

410

Although the PC1 and PC2 are orthogonal by construction and thus correlation between timeseries is zero, after time filtering the PCs timeseries, the modes are correlated (r= 0.41) and the lead-lag correlations with AMOC present a cycle between vertical profiles modes, with a 16 months between the peaks (Fig. ~~11d~~12d). This indicates the limitations of extracting low frequency AMOC-related signals in complex environments using linear methods.

415

High frequency PC1-WB (<2years) represents high frequency density signal at 26N, which could be wind-forced. It is correlated with the AMOC and is independent of the number of years used to identify it (Fig. ~~11e~~12e). Low frequency PC1-WB (>2years) represent a small part of the low frequency density signal at 26N (r<0.2) and it is independent of the number of years (not shown). PC2-WB correlates better with a lower-frequency AMOC signal (>2years) and is also independent of the

420   number of years used to identify it (Fig. ~~11f~~12f).

If we filter the density anomalies prior to performing the EOF, then the leading mode corresponds to PC2-WB seen here. This confirms that we cannot isolate the low frequencies by identifying a deep density signature as works well in NEMO1, therefore time-filtering is needed to identify the inter-annual buoyancy signal in GC2 as a leading mode. Nevertheless, the buoyancy

425   signal is still traceable emerging from the Labrador Sea, and is well captured in PCs, representing relevant information on AMOC variability.

Here we summarise the comparison between density profile modes in different environments as follows:

430   i) In the NEMO1 CTRL simulation with 52 years of data, we are able to find a vertical density pattern at 26N that is buoyancy-forced (i.e. similar to the mode in the BUOY experiment). This has maximum density anomalies at 1500-3000m and corresponds to low-frequency variability of the AMOC. The source is the density changes over the Labrador Sea. In comparison, the leading density mode for the WIND experiment has a maximum at 1000m and represents inter-annual variability of the AMOC.

435

ii) However, if the same methodology is applied over shorter periods, the wind-forced variability dominates both the first 2 EOFs with density anomalies at 1000m and 3000m. The limit for the time-period is about 25 years to extract buoyancy-forced signals that can be related to the AMOC at lower frequencies.

440   iii) When CTRL is compared with the RAPID array PCs, we find similar vertical profiles in the CTRL and observed PCs. Suggesting the short period of RAPID does not allow to extract relevant buoyancy-signals. Wind-forced signals are predominant showing density anomalies that can be also relevant for the geostrophic part of the AMOC at 1000m (but without any lag and at inter-annual scales).

445   iv) The same methodology applied to a more complex GC2 earth system model results in a leading PC that shows positive anomalies between 1000 and 3000m. This PC1 is related to the AMOC at short inter-annual timescales (predominantly wind-forced). The PC2 mode shows reversing density anomalies between 1000 and 3000m and is related to AMOC at lower frequencies (period >2 years). The analysis shows that this PC will be dominant independently from the number of years used in the calculation, although will have less spread for periods longer than ~26 years (Fig. ~~11e~~12e-f).

450

The EOF below 800m method seems to be appropriated to detect buoyancy forced signals from density profiles if we have more than 25 years of data in NEMO1. However, a Lanzcos time filtering for periods > 2years prior to the EOF analysis is recommended in a more complex environments as required for RAPID observations and coupled models. From similarities between NEMO, RAPID and GC2, we conclude that the density profile mode that is most likely buoyancy-forced corresponds

455 to density anomalies at deep levels (3000m) that covary negatively with density anomalies at upper levels (1000m). Timeseries should be filtered with periods >2years and PC correlates with AMOC at 26N 1000m at same frequencies.

7 Discussion

In this work we have used model output and statistical methods to identify vertical density profiles along the boundaries that
460 are consistent with the buoyancy-forced variability. We have shown that the most relevant profile at 26N is found at the WB
using EOF analysis after truncating the density profile from 800m (PC1-WB). This truncation is very effective in emphasising
low frequency (decadal time-scales) signals and in NEMO1 negates the need for temporal filtering, which can also add spurious
signals or lead to excess smoothing. Caveats that warrant further discussion include the differences between the EOFs in
NEMO1 and GC2, and the role of the EB.
465

We note that vertical profile of the WB EOFs in GC2 and NEMO1 are different, especially in the top 1500m, and the
frequencies of the dominant variability in boundary signals in GC2 are higher than the decadal signature seen in NEMO1. We
noticed that shallow (<1500m) density signal related to PC1-WB in NEMO have different timing in CTRL and BUOY
experiments at the tropics (Fig. S5-6), suggesting that at 26N wind forcing is modulating the buoyancy-forced density signal
470 in CTRL. This is also an argument to suggest that in GC2 the shallow signal is more probably wind-forced signal.

Although PCs GC2 contains the low-frequency AMOC-related variance it is perhaps not surprising that the details of the WB
EOFs are different between GC2 and NEMO1 given the range of AMOC variability in models (Biastoch et al., 2008; Cabanes
et al., 2008; PA14; Ortega et al., 2017). The 1° horizontal resolution, and even the ¼° model, may still be too coarse to correctly
475 capture propagating boundary signals (Johnson and Marshall, 2002; Getzlaff et al., 2005; Hodson and Sutton, 2012) from the
Labrador Sea. Therefore, we may not expect the exact details of the boundary density EOFs, or the phase speeds nor the phase
lags identified from the boundary and Labrador Sea signals to be very realistic. Nevertheless, the methods reveal, in two very
different modelling environments, boundary signals consistently related to the geostrophic AMOC at 26N simultaneously.

480 Regarding the differences in the phase speed propagation in NEMO1 and GC2, there are factors that influence propagation
(and hence the phase speed) of boundary waves in numerical models such as i) model resolution (Hsieh et al., 1983; Hodson
and Sutton, 2012). ii) Lateral viscosity (Davey et al., 1983). iii) Orientation of the coastal boundary relative to the ocean grid
(Schwab and Beletsky, 1998). iv) ocean stratification along the trajectory. v) Additionally, complexity in a coupled model in
comparison with an ocean-only model, potentially influences the propagation. We think that both, resolution and complexity
485 are explaining the differences in the phase speed along boundaries shown in the hovmuller plots (Figures 7 and 11), however,
specific sensitive experiments should be designed and performed in order to properly understand these factors.

It is worth noticinge that, due to noise from high frequency wind-forcing, time filtering is needed to see a clear signal due to
noise from high frequency wind-forcing in GC2. Wind forcing can be projected onto density anomalies at deep levels (as it is
490 seen in RAPID data and GC2), it is possible that in the observations similar time-filtering would be needed in order to extract

16

the buoyancy-forced signals. Understanding the differences between these boundary density EOFs between models, would be useful to interpret observations as the record becomes longer, and it should be a focus of further work.

In Section 3.3, we tested the value of using WB and EB together in a single EOF. The fact that the combining the WB and EB at different lags in a singular structure does not improve the explained variance of the EOF WB alone reveals that the WB contains most of the variability at decadal time-scales. This is in agreement with previous results by PA14 and also with the propagating signal from the Labrador Sea that can reach the subtropics along the WB (as in shown by Jackson et al., 2016), but the propagation up the EB is less clearit is not that obvious for the EB. However, we must be clear that we are not saying that EB observations do not make up an important component of the RAPID array observations. Indeed, it has already been shown in observations (Kanzow et al, 2010; Duchez et al 2011), and in models (PA14), that the EB is important for understanding the wind-forced variability in the observed AMOC at 26N from sub-annual to inter-annual time-scales. Indeed, in our own study the use of the EB was important to isolate the density propagation at 3000m depth which is an AMOC-related signature. Therefore, the EB observations are still important in understanding the role of decadal-buoyancy forced variability.

We have found density variability in RAPID which the models suggest could be buoyancy forced at high latitudes (PC1 WB in NEMO1). However, the temporal variabilityThe temporal variability in RAPID WB density modes suggests that wind forcing is still dominating at these short timescales. We have to wait for more years of RAPID data, which could allow the buoyancy forced variance to dominate this mode or give this mode EOF1 status in the decomposition. Although it may be helpful to do some time filtering which could allow buoyancy forced signal to be found in shorter periods of data, the continuation of the RAPID array would be crucial in order to understand the wind-forced inter-annual variability and also the link between the subpolar North Atlantic and the AMOC at 26N.

8 Conclusions

In this work we have used NEMO1 OGCM experiments which separate buoyancy and wind forced signals (BUOY and WIND experiments; Polo et al., 2014), together with statistical techniques, to develop methods to extract the Atlantic boundary density profile signatures at 26N most associated with the buoyancy-forced AMOC signals from an experiment with both buoyancy and wind forced variability (CTRL). After finding the "best" vertical profile on the western boundary, we describe the temporal-spatial structures related to this signal. The main findings are summarized as follows:

- Using EOF analysis and outputs from OGCM experiments we find that the vertical density structure at both the western (WB) and eastern boundaries (EB) at 26N show characteristic signaturescharacteristics that can be unambiguously linked to buoyancy-forcing in the Labrador Sea.

- The vertical structure associated with the leading EOF mode of density variability on the WB (EOF1-WB) shows positive anomalies from 1500 to 3000m depth that can be related to earlier changes in the North Atlantic deep water formation, and to density anomalies over the Labrador Sea, which are seen to lead PC1-WB by ~30 months. The PC1-WB is found to be very robust in both the CTRL and BUOY experiments, signalling buoyancy-forced AMOC variability on decadal timescales. PC1-WB explains 40% and 70% of the density variance for the CTRL and BUOY experiments respectively.

- The PC1-WB is found to lead density anomalies at 1000-1500m on the EB (associated with PC1-EB) by ~7months. The result of combining both boundaries into a single EOF allows to extract the correlated variance and the optimal lag between the boundaries. The combined EOF variance shows maxima when lagging the EB between 7 months and 3 years. This lagged relationship is consistent with density propagation at 2700-3000m.

- In the CTRL experiment, density anomalies at 2000-3000m propagate southwards along the WB and eastward along the Equator and then up to the African coast impacting the vertical structure on both boundaries at 26N. The propagation is continuous from the Labrador Sea around the basin and up to the British Isles. This density signal propagates at a speed ~0.3m/s consistent with the propagation speeds in the BUOY experiment.

- The same method is applied to the RAPID array data for the common period with NEMO1 simulation. The two leading EOFs for the WB have anomalous densities at 1000m and 3000m respectively and are well simulated by the CTRL experiment (Fig. 89). This inter-annual variability is unequivocally wind-forced. The observational record has to be longer in order to identify the buoyancy-forced vertical anomalies, which are more low-frequency signals.

- The same method was able to extract boundary signals from the higher resolution model HadGEM3-GC2. Despite the greater complexity in GC2, the vertical density profiles on the WB at 26N can be clearly related to the geostrophic AMOC although some time-filtering is needed in order to separate the time-scales.

- After filtering (periods below and above of 2 years), PC1-WB is found to be more related to AMOC at 1000m (2000-3000m) at high (low) frequency with a EOF profile with positive density anomalies at 1000m and 3000m. PC2-WB is also related to AMOC at 1000m at low frequency and shows positive (negative) density anomalies at deep 1000m (3000m) level.

- We also show clear density propagation from the Labrador Sea around the basin to the British Isles along a wave track (defined by 3138m bathymetry) at 3000m depth level, which it is also explaining part of the AMOC variability. However, temporal filtering is needed to make this stand out above the noise.

560

- We conclude that the buoyancy-forced signal over the density profile at 26N will be captured in the observations (as well as in coupled models) if the available time period is long enough (>26 years), selecting density profiles with opposite anomalies at 1000m and 3000-3500m, with time filtering of periodicity >2 years, which would help to eliminate high frequency wind-driven signals.

565

19

Author contribution

IP has made the calculations with the data from numerical simulations and observations. IP, JR and KH have analysed the results and IP prepared the manuscript and all authors have contribute to the writing and editing the manuscript.

Competing interests

The authors declare that they have no conflict of interest.

Code and data availability

The code used for the analysis is done in Matlab and it could be available by request to the first author. The data for the three forced experiments belongs to ECMWF and it could be available by request. GC2 data belongs to MetOffice and it could be available by request. RAPID data is fully available online at: http://www.rapid.ac.uk.

Acknowledgments

References

Balan Sarojini, B., Gregory, J.M, Tailleux, R., Bigg, G. R., Blaker, A. T., Cameron, D. R., Edwards, N. R., Megann, A. P., Shaffrey, L.C., and Sinha, B.: High frequency variability of the Atlantic Meridional Overturning Circulation. Ocean Sci., 7, 471–486, 2011 www.ocean-sci.net/7/471/2011/ doi:10.5194/os-7-471-2011, 2011.

Balmaseda, M. A., Mogensen, K., and Weaver, A. T.: Evaluation of the ECMWF ocean reanalysis system ORAS4 Q. J. R. Meteorol. Soc. 139: 1132–1161, 2013.

20

Biastoch, A., Boning, C. W., Getzlaff, J., Molines, J. M., and Madec, G.: Causes of interannual–decadal variability in the meridional overturning circulation of the midlatitude North Atlantic Ocean. J. Climate, 21, 6599–6615, doi:10.1175/2008JCLI2404.1, 2008.

600 Blake, A.T, Hirschi, J. M., McCarthy, G., Sinha, B., Taws, S., Marsh, R., Coward, A., and de Cuevas, B.: Historical analogues of the recent extreme minima observed in the Atlantic meridional overturning circulation at 26°N. Clim Dyn., 22, 457-473. DOI 10.1007/s00382-014-2274-6, 2015.

Bower, A. S, Lozier, M. S., Gary, S. F. and Boning, C. W.: Interior pathways of the North Atlantic meridional overturning
605 circulation. Nature, 459, 243-247. doi:10.1038/nature07979, 2009.

Bretherton, S. B., Smith, C., and Wallace, J. H.: An inter comparison of methods for finding coupled patterns in climate data. J. Climate, 5, 541–560, doi:10.1175/1520-0442(1992)005,0541:AIOMFF.2.0.CO;2, 1992.

610 Cabanes, C., Lee, T., and Fu, L.vL.: Mechanisms of inter-annual variations of the meridional overturning circulation of the North Atlantic Ocean. J. Phys. Oceanogr., 38, 467–480, doi:10.1175/2007JPO3726.1, 2008.

Cunningham, S. A., and Coauthors: Temporal variability of the Atlantic meridional overturning circulation at 26.58N. Science, 317, 935–938, doi:10.1126/science.1141304, 2007.
615
Davey, M. K., Hsieh, W. W., Wajsowicz, R. C.: The Free Kelvin Wave with Lateral and Vertical Viscosity. J. Phys. Oceanogr. 13(12):2182–2191, doi:10.1175/1520-0485(1983)013%3C2182:TFKWWL%3E2.0.CO;2, 1983.

620 Deans, S. R.: The Radon Transform and Some of Its Applications. John Wiley and Sons, 289 pp., 1983.

Dee, D. P., and Coauthors: The ERA-Interim reanalysis: Configuration and performance of the data assimilation system. Quart. J. Roy. Meteor. Soc., 137, 553–597, doi:10.1002/qj.828, 2011.

625 Duchez, A., Frajka-Williams, E., Castro, N., Hirschi, J. M., and Coward, A.: Seasonal to Interannual variability in density around the Canary Islands and their influence on the Atlantic meridional overturning circulation at 26N. J. Geophys. Res. Oceans, 119, 1843-1860. Doi:10.1002/2013JC009416, 2013.

21

Getzlaff, J., Böning, C. W., Eden, C., and Biastoch, A.: Signal propagation related to the North Atlantic overturning, Geophys. Res. Lett., 32, L09602, doi:10.1029/2004GL021002, 2005.

Hermanson, L., Eade R., Robinson, N. H., Dunstone, N., Andrews, M. B., Knight, J. R., Scaife, A. A., and Smith, D. M.: Forecast cooling of the Atlantic subpolar gyre and associated impacts. Geophys. Res. Lett. 41, 5167-5174, 2014.

Hermanson, L., Dunstone, N., Haines, K., Robson, J., Smith, D., and Sutton, R. T.: A Novel transport assimilation method for the Atlantic meridional Overturning Circulation at 26N. Q. J. Roy. Met. Soc. Doi: 10.1002/qj2321, 2013.

Hirschi, J. H., Killworth, P.D., and Blundell, J. R.: Subannual, seasonal, and interannual variability of the North Atlantic meridional overturning circulation. J. Phys. Oceanogr., 37, 1246–1265, doi:10.1175/JPO3049.1, 2007.

Hodson, D. L. R., and Sutton, R.T.: The impact of resolution on the adjustment and decadal variability of the Atlantic meridional overturning circulation in a coupled climate model. Climate Dyn., 39, 3057–3073, doi:10.1007/s00382-012-1309-0, 2012.

Hsieh, W. W., Davey, M. K., Wajsowicz, R. C.: The Free Kelvin Wave in Finite-Difference Numerical Models. J. Phys. Oceanogr., 13(8):1383–1397, doi: 1510.1175/1520-0485(1983)013%3C1383:595 TFKWIF%3E2.0.CO;2, 1993.

Huang, R. X., Cane, M. A., Naik, N., and Goodman, R.: Global adjustment of the thermocline in response to deepwater formation. Geophys. Res. Lett., 27, 759-762, 2000.

Illig, S., Dewitte, B., Ayoub, N., du Penhoat, Y., Reverdin, G., De Mey, P., Bonjean, F., and Lagerloef, S. G.: Interannual long equatorial waves in the tropical Atlantic from a high-resolution ocean general circulation model experiment in 1981 – 2000. J. Geophys. Res., 109, C02022, doi:10.1029/2003JC001771, 2004.

Jackson, L. C., Peterson, K. A., Roberts, C. D., and Wood, R. A.: Recent slowing of Atlantic overturning circulation as a recovery from earlier strengthening. Nature Geosience, DOI: 10.1038/NGEO2715, 2016.

Johnson, H. L and Marshall, D. P.: A theory for the surface Atlantic response to thermohaline variability. J. Phys. Oceanogr., 32, 1121-1132, 2002.

Kawase, M.: Establishment of deep ocean circulation driven by deep-water production, J. Phys. Oceanogr., 17, 2294 – 2317, 1987.

Kanzow, T., Cunningham, S. A., Johns, W. E., Hirschi, J. M., Marotzke, J., Baringer, M. O., Meinen, C. S., Chidichimo, M. P., Atkinson, C., Beal, L. M., Bryden, H. L., and Collins, J.: Seasonal variability of the Atlantic meridional overturning circulation at 26.58N. J. Climate, 23, 5678–5698, doi:10.1175/2010JCLI3389.1, 2010.

Karspeck, A. R., Stammer, D., Köhl, A., Danabasoglu, G., Balmaseda, M., Smith, D. M., Fujii, Y., Zhang, S., Giese, B., Tsujino, H., Rosati, A.: Comparison of the Atlantic meridional overturning circulation between 1960 and 2007 in six ocean reanalysis products, Climate Dynamics, doi:10.1007/s00382-015-278, 2015.

Knight, J. R., Allan, R. J., Folland, C. K., Vellinga, M., and Mann, M. E.: A signature of persistent natural thermohaline circulation cycles in observed climate. Geophys. Res. Lett., 32, L20708, doi:10.1029/2005GL024233, 2005

Lanczos, C.: Applied Analysis. Prentice-Hall 539 pp., 1956.

Marshall, D., and Johnson, H.: Propagation of meridional circulation anomalies along western and eastern boundaries. J. Phys. Oceanogr., 43, 2699-2717. . DOI:10.1175/JPO-D-13-0134.1, 2013.

McCarthy, G.D., Smeed, D.A., Johns, W.E., Frajka-Williams, E., Moat, B.I., Rayner, D., Baringer, M.O., Meinen, C.S., Collins, J. and Bryden, H. L.: Measuring the Atlantic Meridional Overturning Circulation at 26N. Progress Oceanogr. 130, 91-111, 2015.

Megann, A., Storkey, D., Aksenov, Y., Alderson, S., Calvert, D., Graham, T., Hyder, P., Siddorn, J., and Sinha, B.: GO5.0: the joint NERC–Met Office NEMO global ocean model for use in coupled and forced applications. Geosci. Model Dev., 7, 1069–1092. doi:10.5194/gmd-7-1069-2014, 2014.

Menary, M. B., Hodson, D. L. R., Robson, J., Sutton, R. T., Wood, R. A., and Hunt, J. A.: Exploring the impact of CMIP5 model biases on the simulation of North Atlantic decadal variability, Geophys. Res. Lett., 42, doi:10.1002/2015GL064360, 2015.

Metz, W.: Optimal relationship of large-scale flow patterns and the barotropic feedback due to high-frequency eddies. J. Atmos. Sci., 48, 1141–1159, 1991.

Ortega, P., Robson, J., Sutton, R. T., and Andrews, M. B.: Mechanisms of decadal variability in the Labrador Sea and the wider North Atlantic in a high-resolution climate model. Clim. Dyn., doi: 10.1007/s00382-016-3467-y, 2017.

23

Pillar, H. R, Heimbach, P., Johnson, H. L., Marshall, D. P.: Attributing variability in Atlantic meridional overturning to wind and buoyancy forcing. J. Climate DOI: http://dx.doi.org/10.1175/JCLI-D-15-0727.1, 2016.

Polo, I., Robson, J., Sutton, R. T., and Balmaseda, M.: The importance of wind and buoyancy forcing for the boundary density variations and the geostrophic component of the AMOC at 26N. J. Phys. Oceanogr., 44, 2387-2408. DOI: 10.1175/JPO-D-13-0264.1, 2014.

Polo, I., Lazar A., Rodriguez-Fonseca, B., and Arnault, S.: Oceanic Kelvin waves and tropical Atlantic intraseasonal Variability: 1. Kelvin wave characterization, J. Geophys. Res., 113, C07009, doi:10.1029/2007JC004495, 2008.

Roberts, C. D. and coauthors: Atmosphere drives recent interannual variability of the Atlantic meridional overturning circulation at 26.58N. Geophys. Res. Lett., 40, 5164–5170, 2013.

Robson J., Polo, I., Hodson, D. L. R., Stevens, D. P., and Shaffrey, L. C.: Decadal prediction of the North Atlantic subpolar gyre in the HiGEM high−resolution climate model. Clim. Dyn., DOI 10.1007/s00382-017-3649-2, 2017.

Robson J., Ortega, P., and Sutton, R. T.: A reversal of climatic trends in the North Atlantic since 2005. Nature Geoscience, DOI: 10.1038/NGEO2727, 2016.

Robson, J., Hodson, D. L. R., Hawkins, E., and Sutton, R. T.: Atlantic overturning in decline? Nature Geosci. 7, 2-3, 2014.

Robson, J., Sutton, R. T., and Smith, D. M.: Initialized predictions of the rapid warming of the North Atlantic Ocean in the mid 1990s. Geophys. Res. Lett. 25,L19713, 2012.

Roussenov, V. M., Williams, R. G., Hughes, C. W., and Bingham, R. J.: Boundary wave communication of bottom pressure and overturning changes for the North Atlantic. Journal of Geophysical Research, 113(C8), C08042, 2008.

Schwab, D. J., and Beletsky, D.: Propagation of Kelvin waves along irregular coastlines in finite-difference models. Advances in Water Resources, vol 22, 239-245. https://doi.org/10.1016/S0309-1708(98)00015-3, 1998.

Smeed, D. A., Josey, S. A., Beaulieu, C., Johns, W. E., Moat, B. I., Frajka-Williams, E., and coauthors: The North Atlantic Ocean is in a state of reduced overturning. Geophys. Res. Lett., 45, 1527–1533. https://doi.org/10.1002/2017GL076350, 2018.

Smeed, D. A., McCarthy, G., Rayner, D., Moat, B.I., Johns, W. E., Baringer, M. O., and Meinen, C.S.: Atlantic meridional overturning circulation observed by the RAPID-MOCHA-WBTS (RAPID-Meridional Overturning Circulation and Heatflux Array-Western Boundary Time Series) array at 26N from 2004 to 27th October 2017 Page 2 of 5 2017. British Oceanographic

735   Data Centre - Natural Environment Research Council, UK. doi: 10.5285/5acfd143-1104-7b58-e053-6c86abc0d94b, 2017.

Smeed, D. A., McCarthy, G., Cunningham, S. A., Frajka-Williams, E., Rayner, D., Johns, W. E., Meinen, C. S., Baringer, M. O., Moat, B. I., Duchez, A., and Bryden, H. L.: Observed decline of the Atlantic meridional overturning circulation 2004–2012, Ocean Sci., 10, 29-38, doi:10.5194/os-10-29-2014, 2014.

740

Stepanov, V. N., Haines, K., and Smith, G. C.: Assimilation of RAPID array observations into an ocean model. Quaterly J. Roy. Meteo. Soc., 138 (669). pp. 2105-2117. ISSN 1477-870X doi: 10.1002/qj, 2012.

Sutton, R. T., and B. Dong, B.: Atlantic Ocean influence on a shift in European climate in the 1990s. Nat. Geosci., 5, 788–

745   792, doi:10.1038/ngeo1595, 2012.

Thomas, C. M., and Haines, K.: Using lagged covariances in data assimilation, Tellus A: Dynamic Meteorology and Oceanography, 69:1, 1377589, DOI: 10.1080/16000870.2017.1377589, 2017.

750   Thomson, D. J.: Spectrum estimation and harmonic analysis. Proc. IEEE, 70, 1055–1096, doi:10.1109/PROC.1982.12433, 1982.

Uppala, S. M., and coauthors: The ERA-40 Re-Analysis. Quart. J. Roy. Meteor. Soc., 131, 2961–3012, doi:10.1256/qj.04.176, 2005.

755

von-Storch, H., and Zwiers, F. W.: Statistical Analysis in Climate Research. Cambridge University Press. https://doi.org/10.1017/CBO9780511612336, 1999.

Walters, D. N., Best, M. J., Bushell, A. C., and coauthors: The Met Office Unified Model Global Atmosphere 3.0/3.1 and

760   JULES Global Land 3.0/3.1 configurations. Geosci Model Dev 4:919–941. doi: 10.5194/gmd-4- 919-2011, 2011.

Wang, C., Dong, S. and Munoz, E.: Seawater density variations in the North Atlantic and the Atlantic meridional overturning circulation Clim Dyn (2010) 34:953–968 DOI 10.1007/s00382-009-0560-5, 2010.

765 Williams, K. D., Hill, R., Hinto, T., Shelly, A., Sinha, B., Harris, C. M., Hyder, P., Walters, D. N., Bodas-Salcedo, A., Ineson, S., Masato, G., West, A., Camp, J., Milton, S. F., Woollings, T., Comer, R. E., Roberts, M. J., and Xavier, P. K., Copsey, D., Rowell, D. P., Fereday, D.: The Met Office Global Coupled model 2.0 (GC2) configuration Geosci. Model Dev., 88, 1509–1524, doi:10.5194/gmd-88-1509-2015, 2015.

770 Zhang, R.: Latitudinal dependence of Atlantic Meridional Overturning Circulation (AMOC) variations. Geophys. Res. Lett., 37, L16703. Doi: 10.1029/2010GL044474, 2010.

Zhang, R., Rosati, A., Anderson, W. G., Dixon, K. W., Lee, H. C., and Zeng, F.: Sensitivity of the North Atlantic Ocean Circulation to an abrupt change in the Nordic Sea overflow in a high resolution global coupled climate model. J. Geophys. 775 Res-Oceans, 116, C12024, doi: 10.1029/2011JC007240, 2011.

Table 1. Correlations between PCs f800m and AMOC timeseries in NEMO1. Correlations between the geostrophic AMOC and the PCs at the boundaries for the CTRL and BUOY experiments. ~~Correlations~~Significant correlations are ~~significant when are above 0.3 from~~highlighted with a star based on a t-test at 95% confidence level~~.~~ and after calculating the number of effective degrees of freedom.

Correlation ~~no filter/1yrm~~Nf / 1yrF	PC1-WB AMOC	PC1-EB AMOC	PC1-EB-PC1-WB	
BUOY	0.88*/0.89*	0.80*/0.81*	0.83*/0.84*	

CTRL	0.33*/0.47*	-0.04/0.42*	0.36*/0.67*	

Table 2. Correlations between PCs f800m WB and AMOC timeseries in GC2. Correlations between the geostrophic AMOC and the PCs at the WB for the GC2 experiment. ~~Correlations~~Significant correlations are ~~significant when are above 0.2 from~~highlighted with a star based on a t-test at 95% confidence level~~.~~ and after calculating the number of effective degrees of freedom.

790

Correlation	Nf	< 2 years	>2 years	
PC1-WB, AMOC	0.45*	0.49*	0.25	
PC2-WB, AMOC	0.13	0.06	0.32*	
PC1-WB, PC2-WB	0	0.11	0.32*	
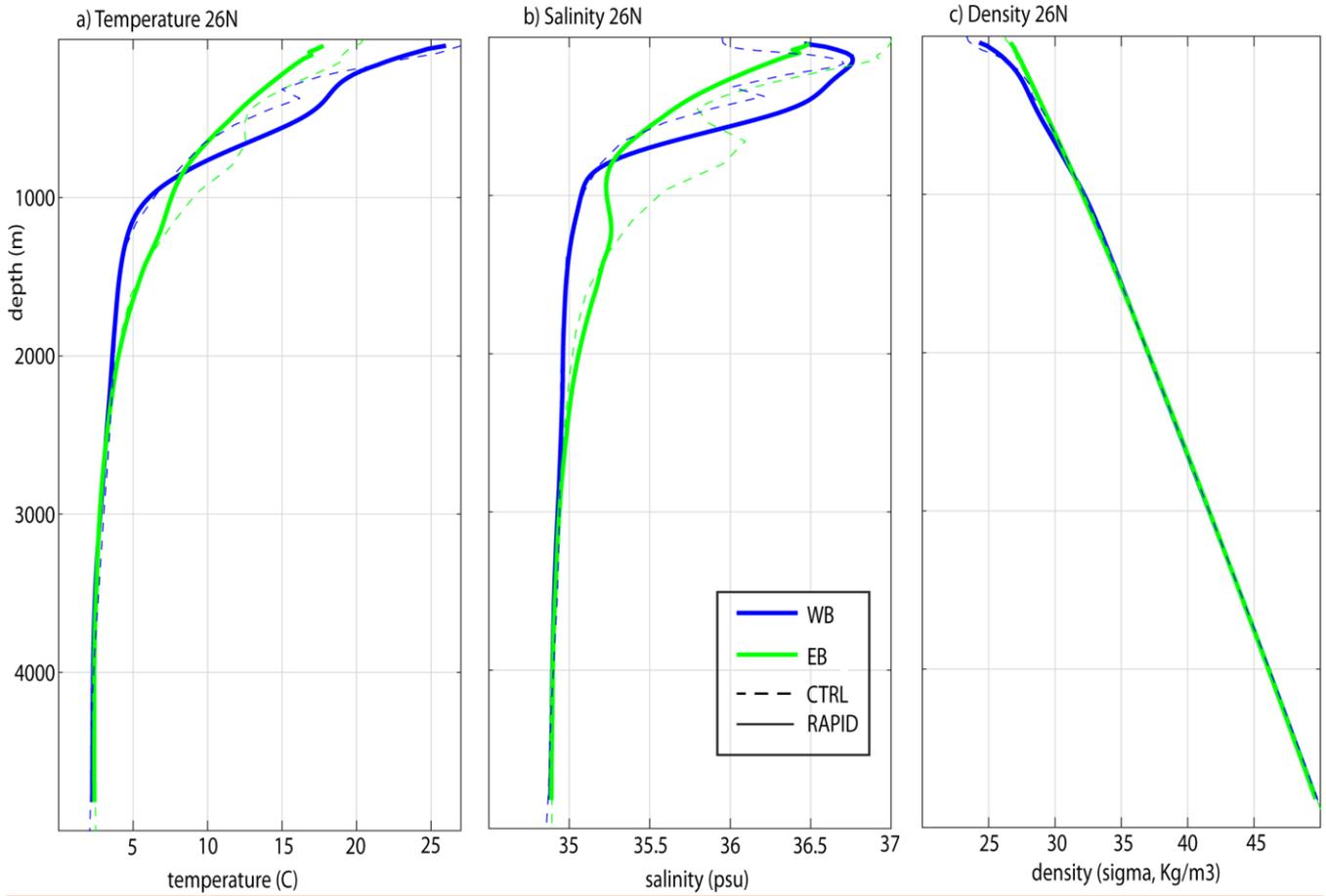
Figure 1. Temperature, salinity and density profiles at 26N. a) Temperature profiles (in ºC) at 26N for WB (blue line) and EB (green line), CTRL experiment (dashed line) and RAPID data (solid line) for the period 2004-2009. b) same as a) but for salinity profiles. c) same

as a) but for the density profiles.

a) AMOC NEMO1 r=0.43

b) AMOC NEMO1 1yrF r=0.62 r=0.86

c) r (density-WB SUM, CTRL)

d) r (density-EB SUM, CTRL)
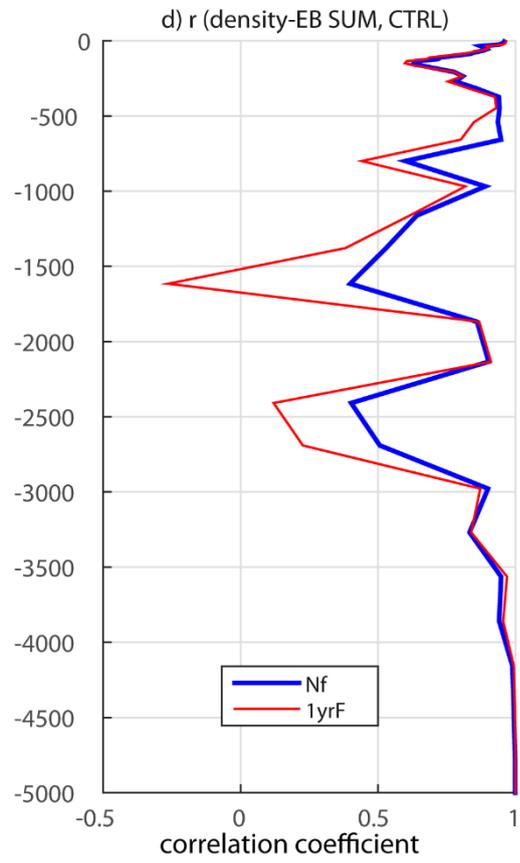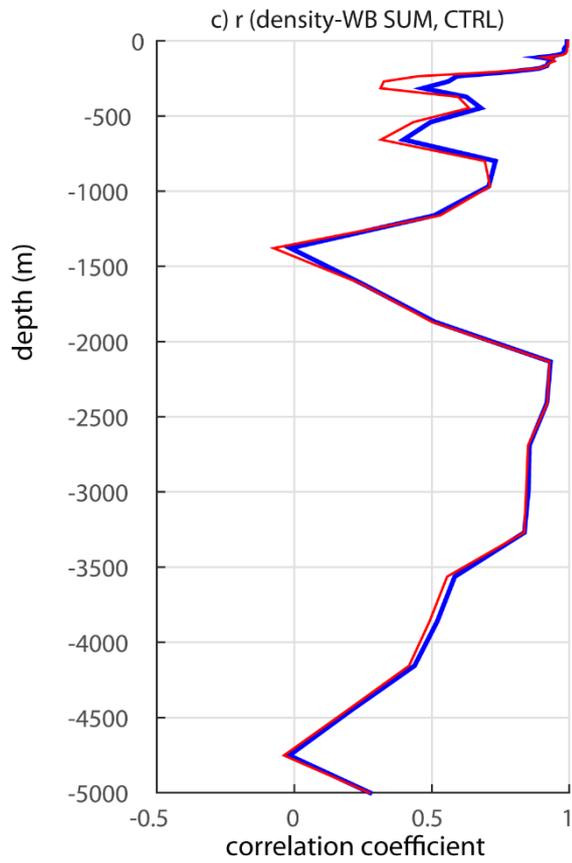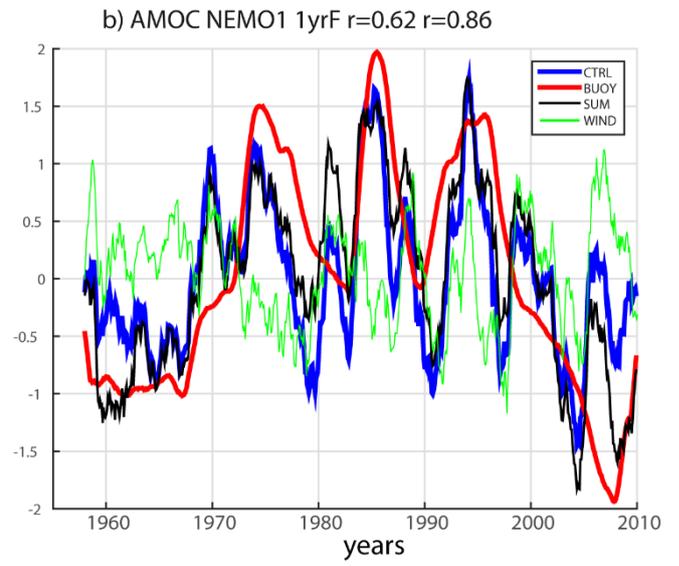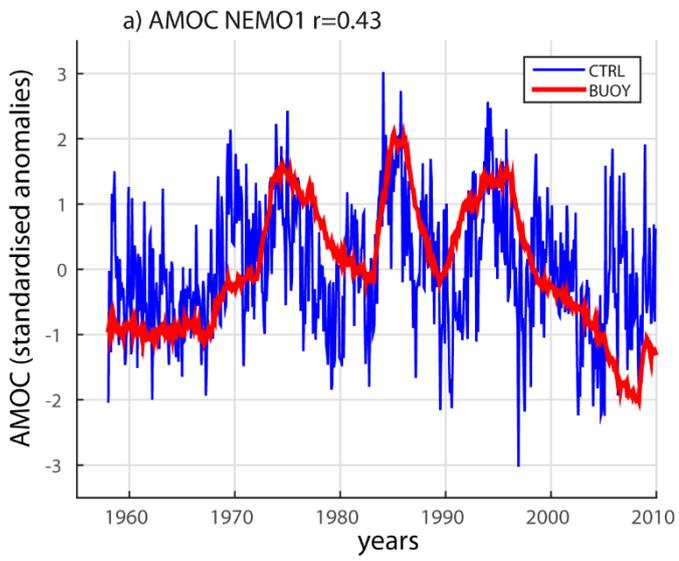
Figure 2. **AMOC and linearity of the forcings for the density profiles at the boundaries.** a) Geostrophic AMOC defined at 26N and 1100m level for the CTRL (blue line) and BUOY (red line) experiments. Timeseries have been de-seasonalised and de-trended and standardised. Correlation in the title corresponds to correlation between ~~blue and red lines.~~both timeseries. b) Same as a) but the timeseries have been smoothed with one-year running mean filter and black line refers to AMOC for the SUM. Green line is the filtered AMOC timeseries for the WIND experiment. In the title, double correlation score corresponds to correlations between blue-red and blue-back lines. c) Correlation coefficient between profiles of density anomalies at the WB for the CTRL experiment and SUM (BUOY+WIND). Blue line refers to anomalies without time filtering, red line refers to anomalies that have been smoothed with one year running mean filter. d) Same as c) but for the EB.
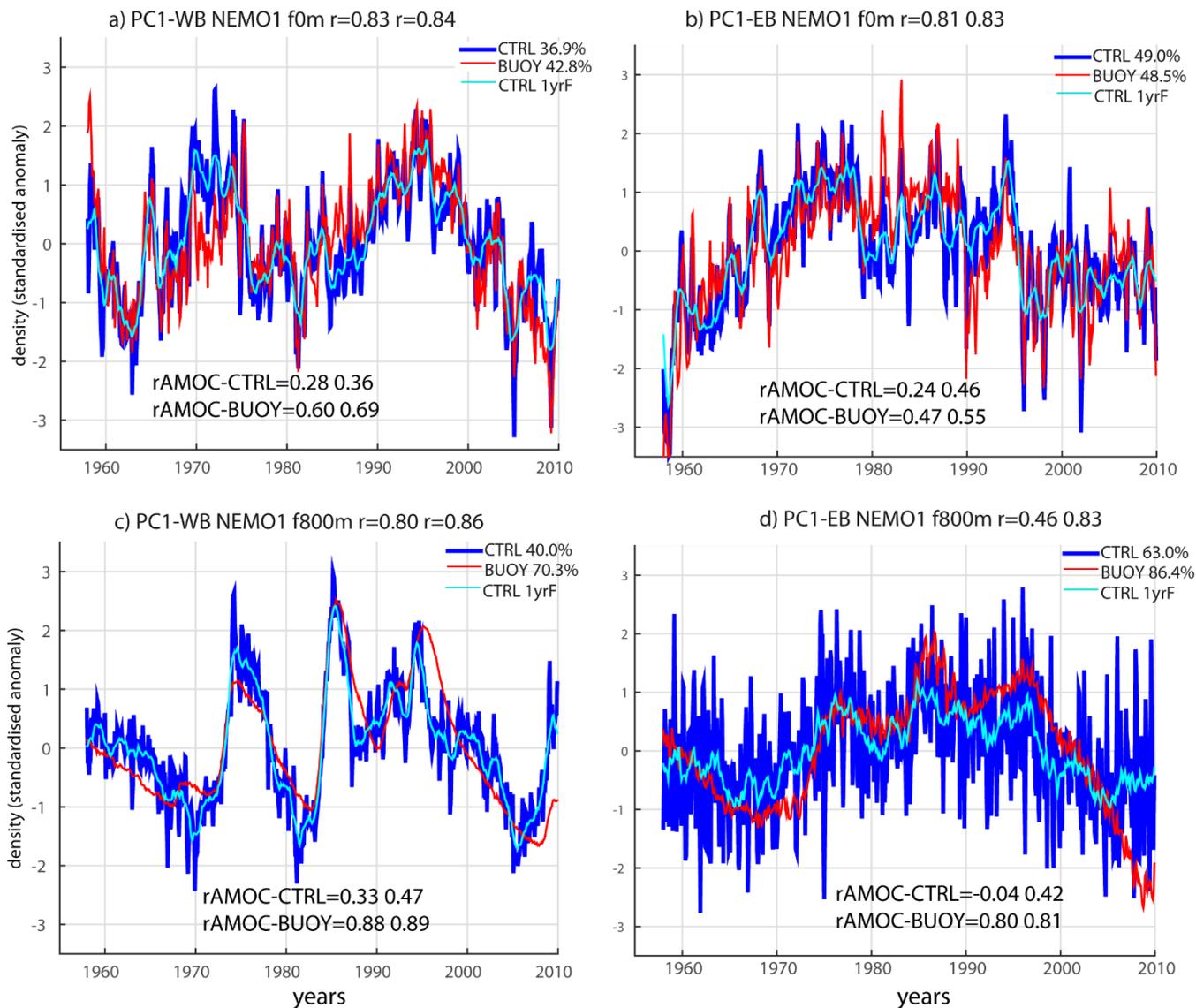
Figure 23 AMOC at 26N and individual EOF of density profiles at the 26N boundaries: sensitivity to depth truncation. a) Timeseries associated with the leading mode of density variability of the water column at the WB-26N for the CTRL (blue line) and BUOY (red line) experiment, considering the total water column. Cyan line corresponds to the time series of the CTRL smoothed with one-year running mean filter. In the title, double correlation score corresponds to correlations between blue-red and blue-cyan lines b) Same as a) but for the EB-26N. c) -d) Same as a)-b) but considering from 800m downwards. All the timeseries are dimensionless and the percentage of explained variance is detailed on the legend as well as the correlation with AMOC timeseries (in Fig. 1a2a-b). The correlation between the CTRL and BUOY experiments timeseries are detailed in the title for the non-filter and the 1y running mean filtering. The EOFs are performed after removing seasonal cycle, linear trend and depth weighting pre-processing is applied.

a) r(AMOC, PC1-WB truncations) CTRL Nf (dashed) 1yrF (solid)

b) r(AMOC, PC1-EB truncations) CTRL Nf (dashed) 1yrF (solid)

AMOC lagging   AMOC leading

lags (months)

c) EOF1-WB f800m NEMO1

d) EOF1-EB f800m NEMO1

depth (m)

density anomalies (Kg/m3)

r CTRL-BUOY=0.80
rCTRL-WIND=0.09

r CTRL-BUOY=0.46
rCTRL-WIND=0.87

CTRL
BUOY
WIND
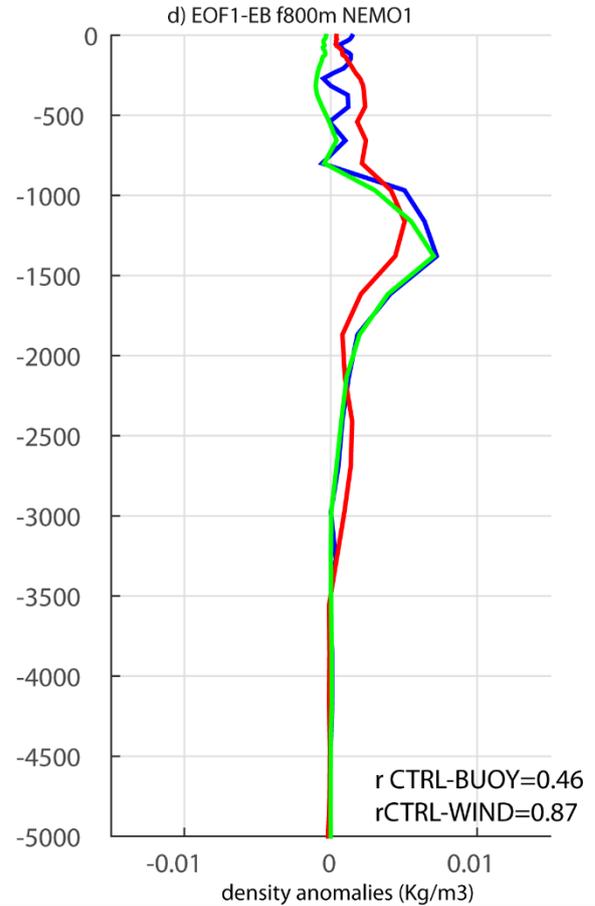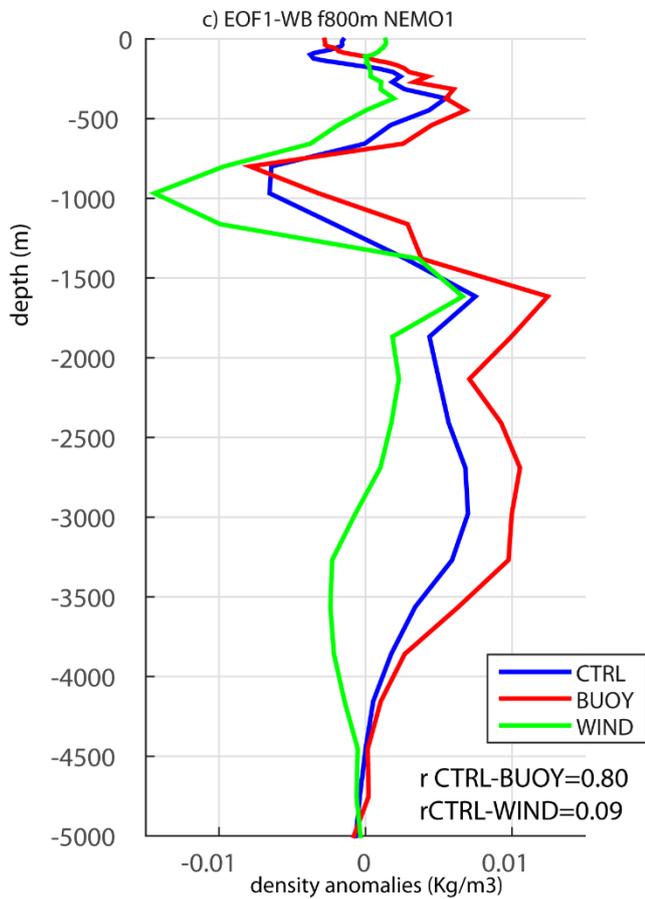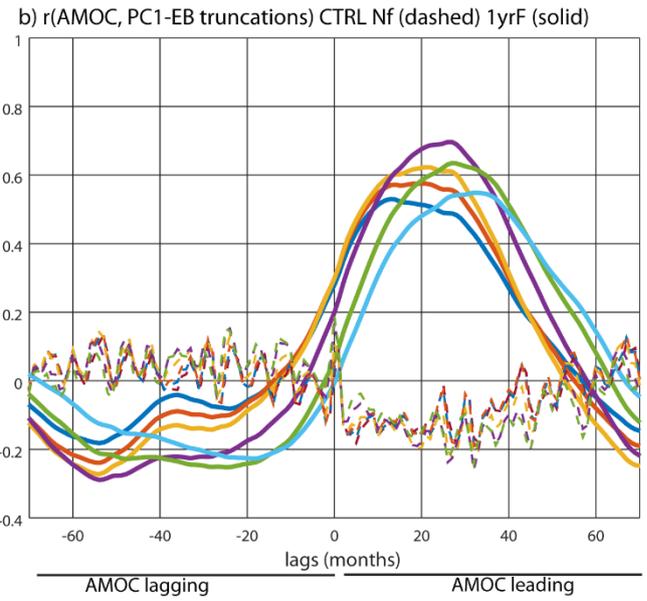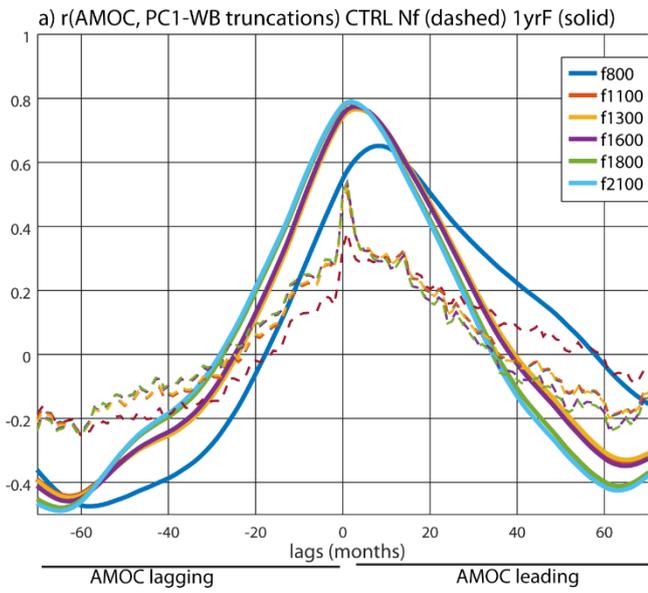
Figure ~~3~~4. Individual EOF of density profiles at the 26N boundaries from 800m. a) Lead-lag correlations between AMOC at 1000m and 1PC-WB at different truncations (represented with different ~~colors~~colours). Positive (negative) values over x-axis represents the AMOC leading (lagging) the PC1-EB. 1-year running mean filter (solid line) and no filter (dashed line) is applied to the timeseries for the CTRL experiment. b) Same as a) but for the correlations between AMOC and PC1-EB. c) Profile of density anomalies (in kg/m³) associated with the leading mode of density variability of the water column from 800m downwards at WB-26N for the CTRL (blue line) and BUOY (red line) and WIND (green line) experiment. Associated timeseries are in Fig. ~~2c~~3c except for the WIND experiments. d) Same as c) but for the EB-26N, associated timeseries are in Fig. ~~2d~~3d except for the WIND experiment. Correlation coefficient between time series of the PCs for CTRL with BUOY and WIND are detailed.
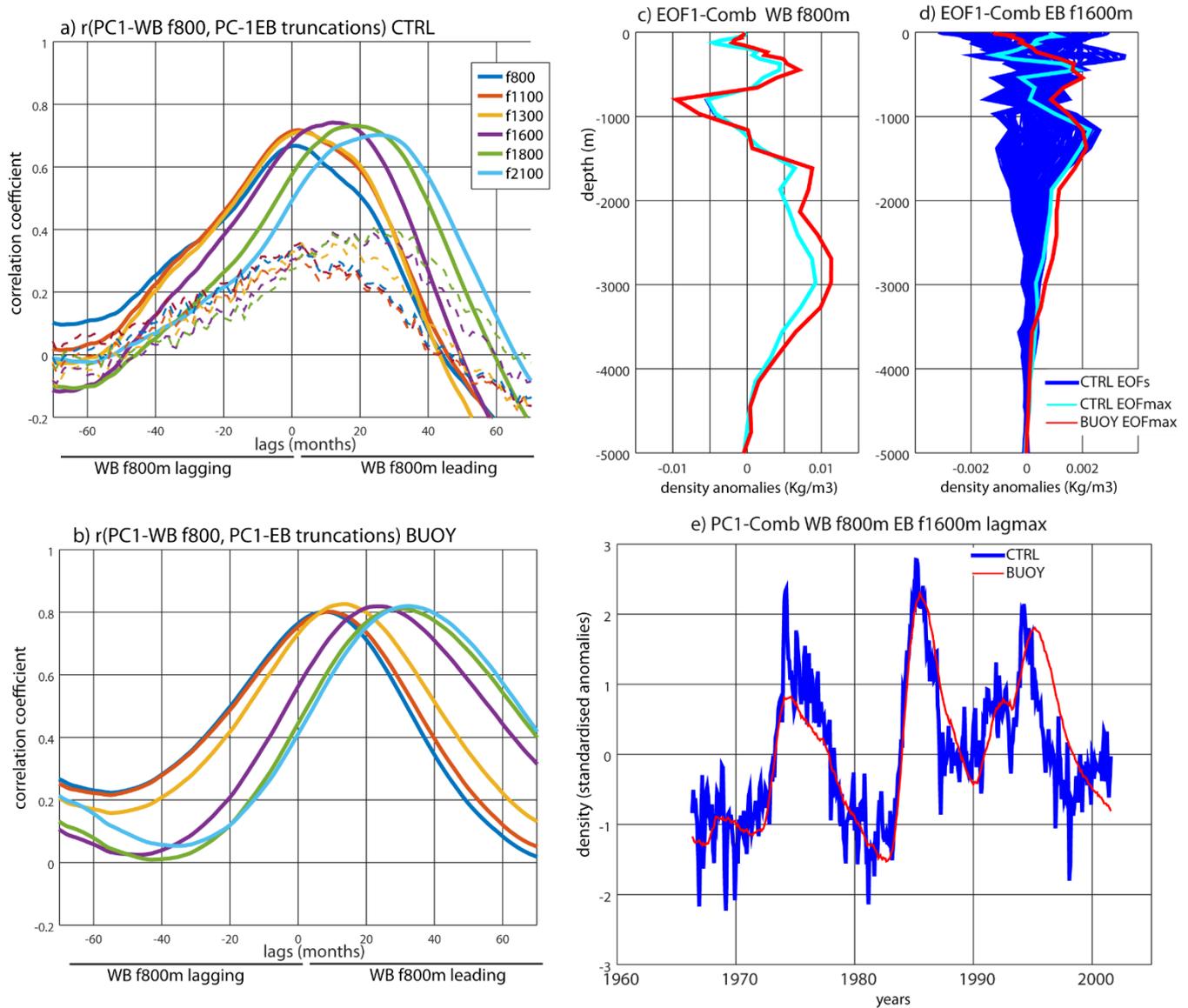
Figure 45. Relationship between Boundaries and combined EOF. a) Lead-lag correlations between PC1-WB from 800m and PC1-EB at different truncations (represented with different ~~colors~~colours). Positive (negative) values over x-axis represents the PC1-WB leading (lagging) the PC1-EB. 1-year running mean filter (solid line) and no filter (dashed line) is applied to the timeseries for the CTRL experiment. b) Same as a) but for the BUOY experiment and only 1-year running mean filter is plotted. c) - d) are the EOFs as the result of combining the density profile at the WB (from 800m) at lag 0 and the EB (from 1600m) at different lags. The CTRL experiment is plotted in blue and the cyan line corresponds to the EOF at the lag in which the explained fraction of variance is maximum (EOFmax). The latter equivalent EOFmax profile for the BUOY experiment is plotted in red. e) The associated timeseries of EOFmax for the CTRL (blue) and BUOY (red) experiment.

a) PC1-WB x den 2700-3000m CTRL -30 months
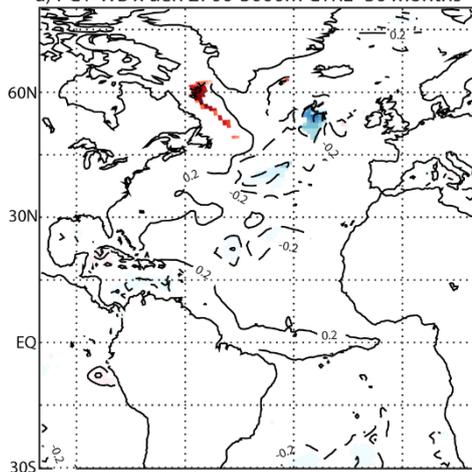
d) PC1-WB x den 2700-3000m BUOY -30 months
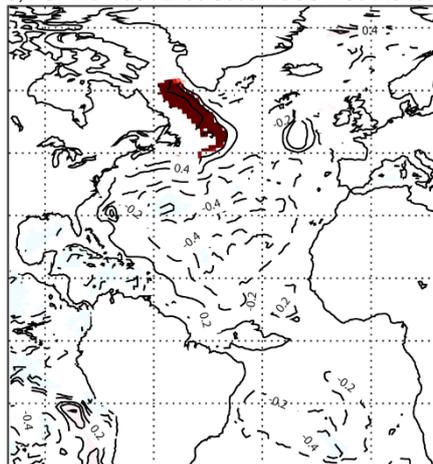
b) PC1-WB x den 2700-3000m CTRL -20 months
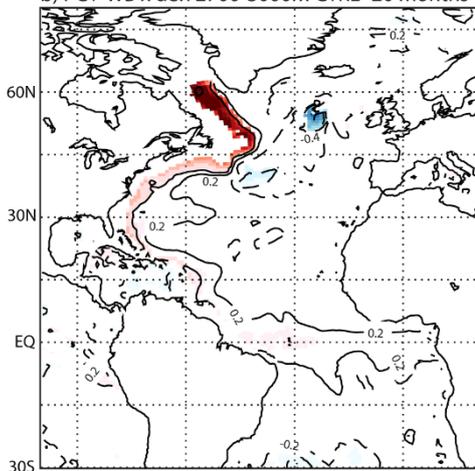
e) PC1WBxspa2700-3000m BUOY -20 months
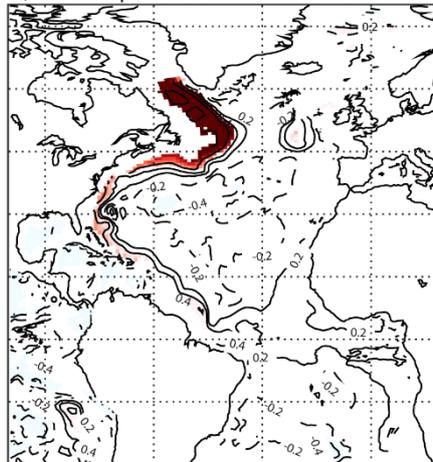
c) PC1-WB x den 2700-3000m CTRL -10 months
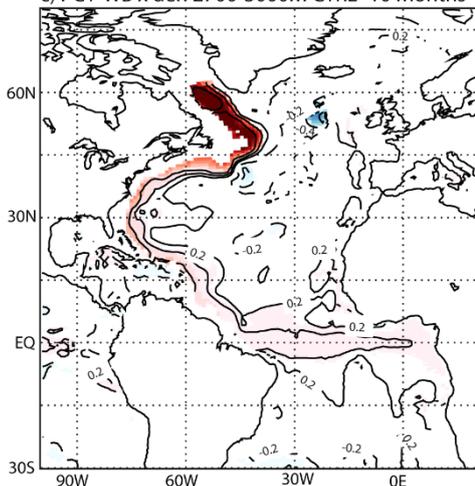
f) PC1-WB x den 2700-3000m BUOY -10 months

density anomalies (Kg/m3)
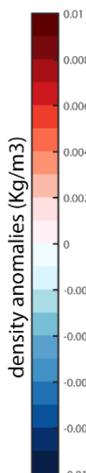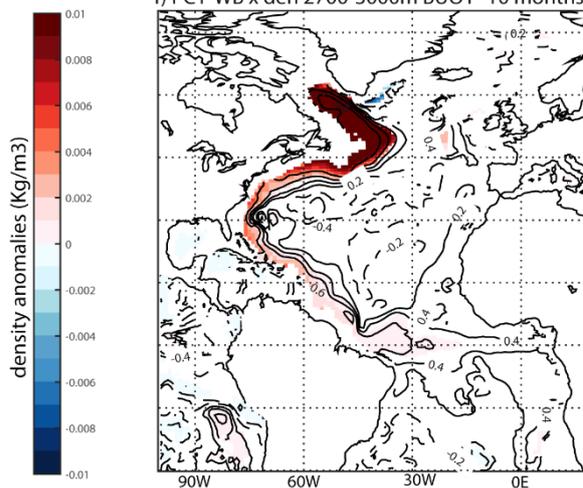
Figure 5̶6. **The spatial relationship of density anomalies with PC1-WB in the CTRL and BUOY experiment.** a) Density anomalies
845   (in kg/m³) averaged from 2700m to 3000m levels, 30 months in advance projected onto PC1-WB (in kg/m³) for the CTRL experiment.
Black lines correspond to the correlation every 0.2. Only significant areas are plotted with a Student's t-test with alpha=0.1at 95%
confidence level considering only effective degrees of freedom according to Metz (1991). b) and c) are same as a) but for lags -20 and -10
months. d)-f) same as a)-c) but for the BUOY experiment.

a) Track points
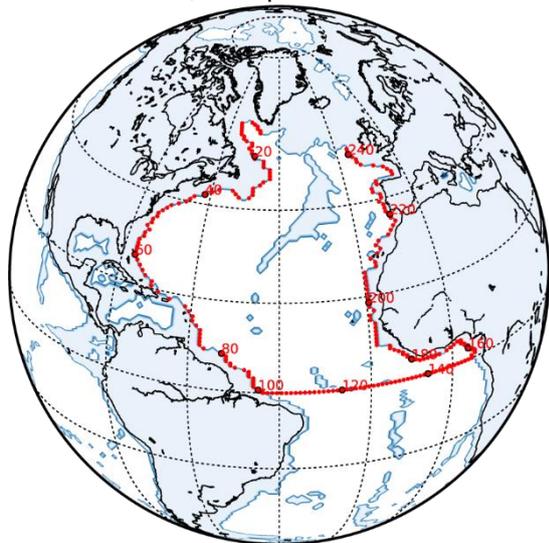
b) Hovmuller (track vs years) den 2700-3000 NEMO1 CTRL
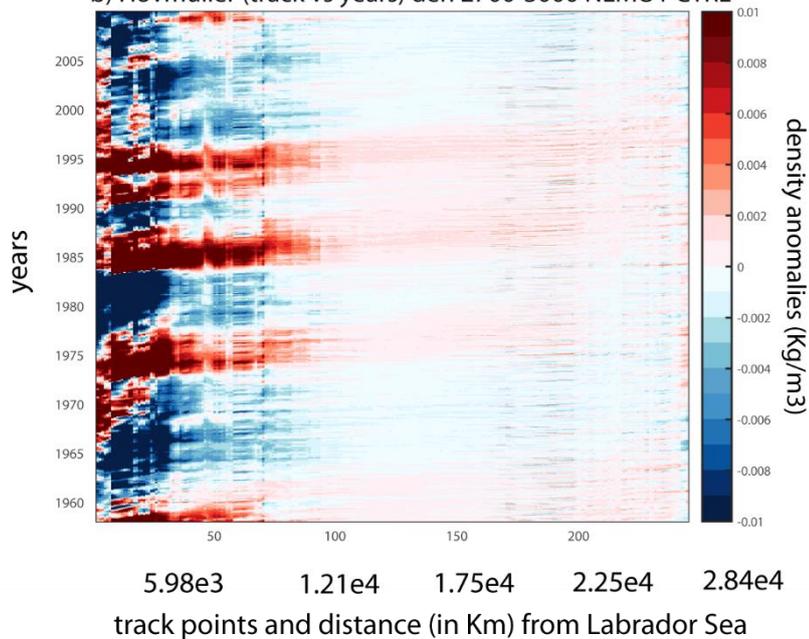
Figure 67. Hovmöller diagrams of density anomalies along the wave-track in the CTRL experiment. a) Map of the wave-track used in the study. The track-points correspond to the first point before the coast following the bathymetry at 3269 m. The points for all depth levels has been tracked. b) Density anomalies (in kg/m³) along the track averaged from 2700m to 3000m levels for the CTRL experiment

39

(in kg/m³).. The anomalies are the result of removing the linear trend and the seasonal cycle. Distance (in km) from Labrador Sea is

855 associated with track-points in the x-axis.
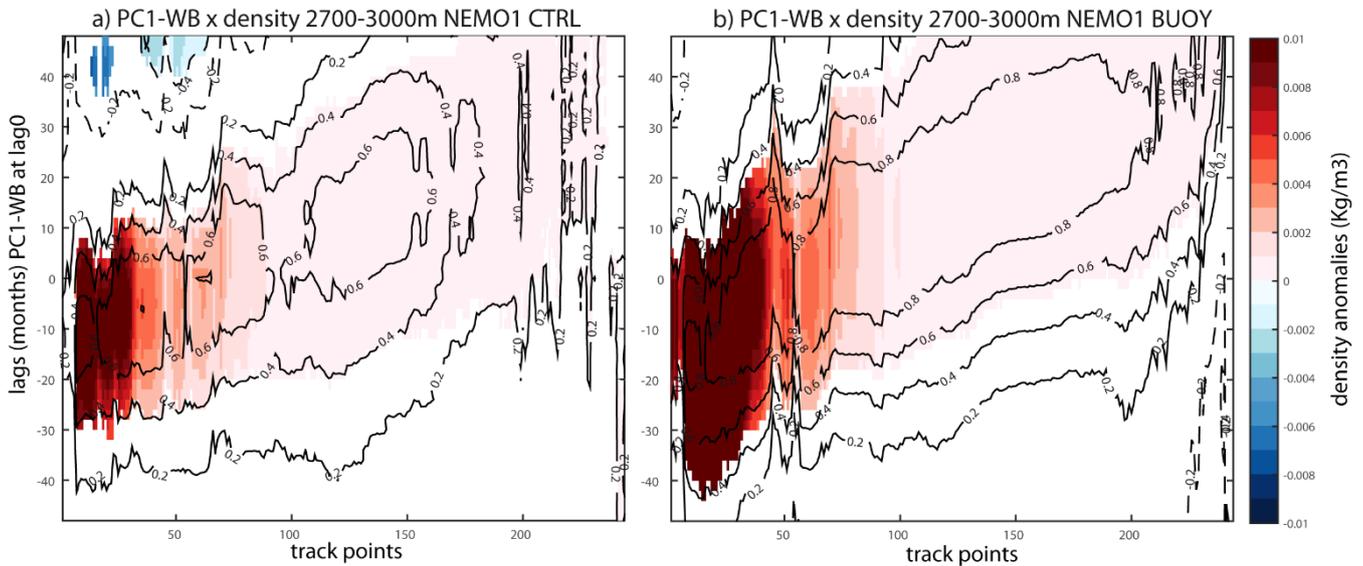
Figure 78. PC1-WB and density along the wave-track. a) Density anomalies (in kg/m³) averaged from 2700m to 3000m projected onto PC1-WB (in kg/m³) for the CTRL experiment. Black lines correspondscorrespond to the correlation every 0.2. Only significant areas are

860 plotted with a Student's t-test with alpha=0.1at 95% confidence level considering only effective degrees of freedom. according to Metz (1990). b) Same as a) but for the BUOY experiment.
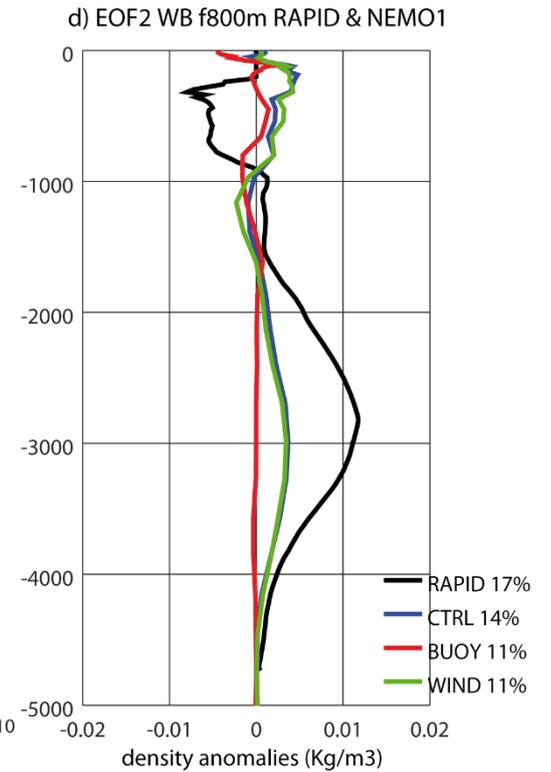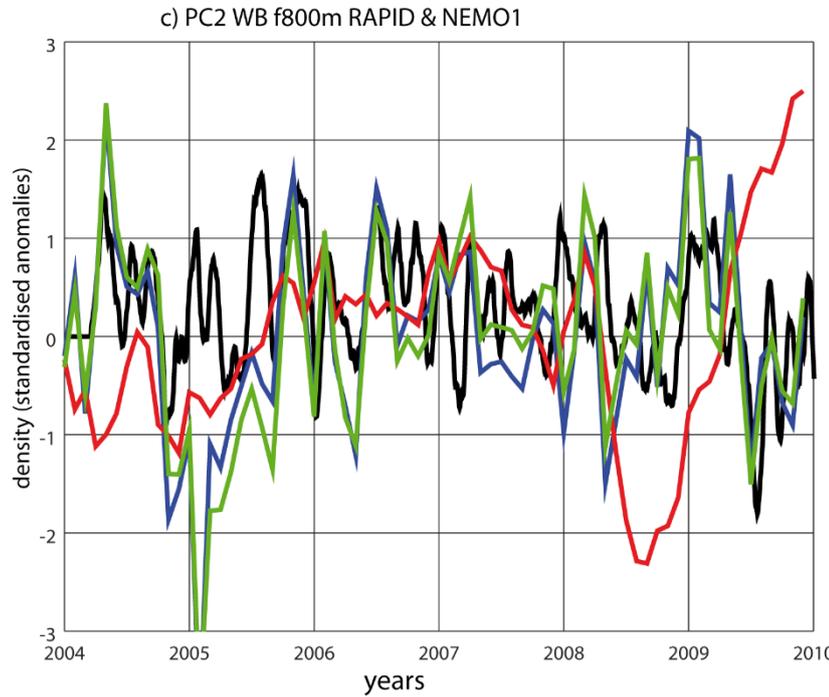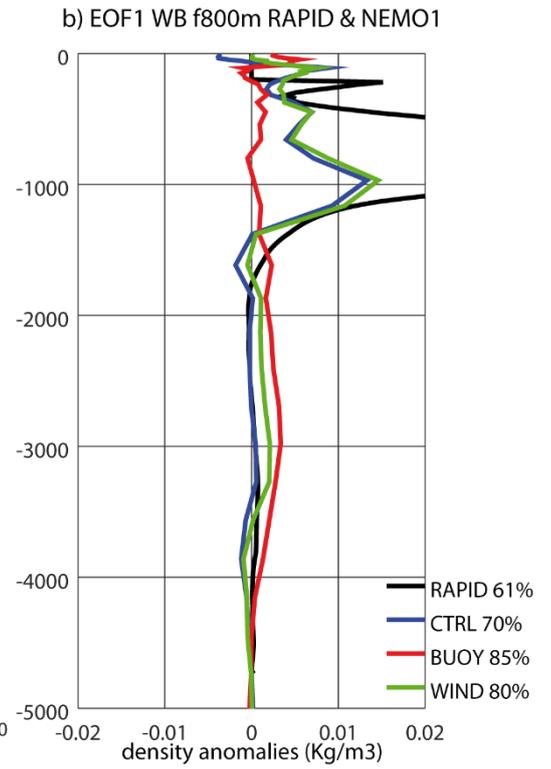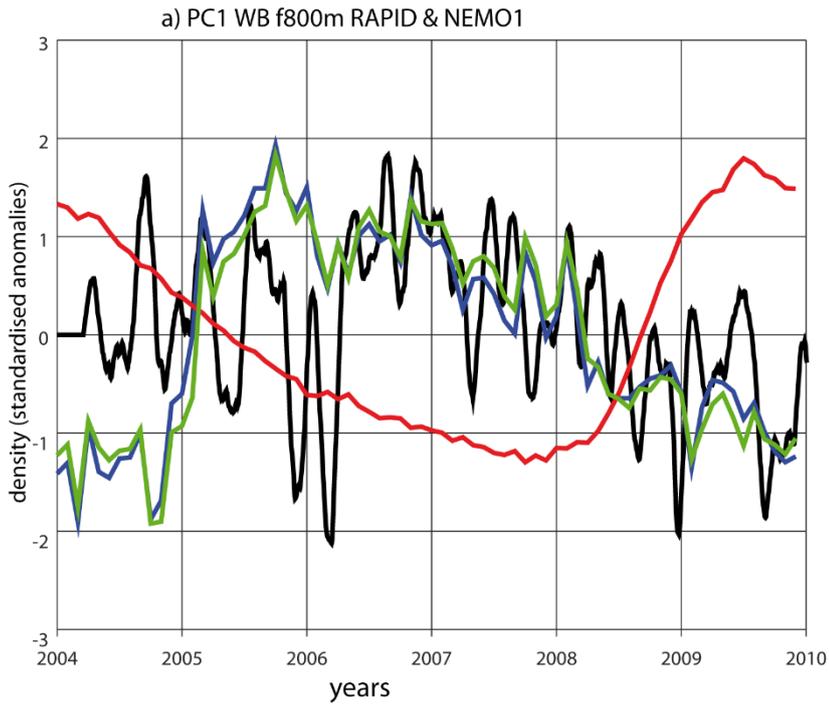
Figure 8~~9~~. **Leading EOFs for the RAPID data and NEMO experiments**. a) ~~Pcs Time series~~PCs Timeseries associated with the leading EOF for the WB-26N for the RAPID array (black line), the CTRL (blue line), BUOY (red line) and WIND (green line) ~~and BUOY (red line)~~ experiments for the common period 2004-~~2010~~2009. b) EOF patterns linked to PC in a). c) -d) Same as a) -b) but for the second mode. For the period 2004-~~2010~~2009 the EOFs for the CTRL experiment captures wind-forced only modes.
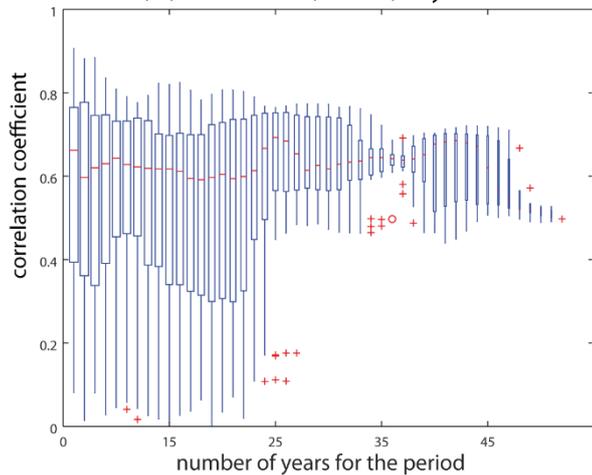
42

a) r(PC1-WB CTRL, PC1-WB WIND)
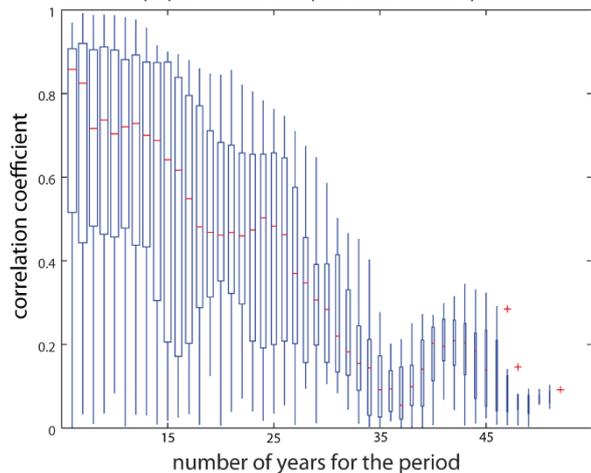
b) r(PC1-WB CTRL, PC1-WB BUOY)
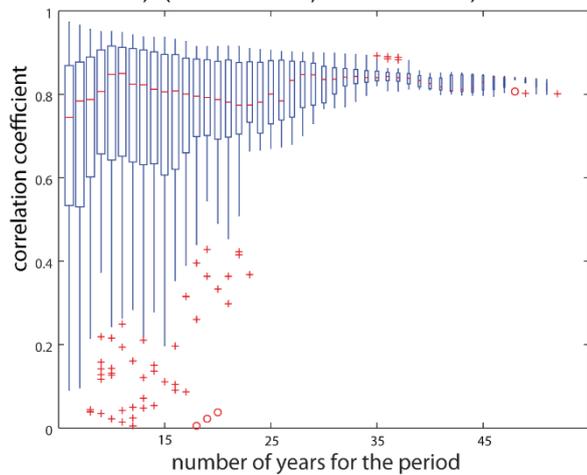
c) r(PC1-WB CTRL, AMOC) >2yr

870 **Figure ~~9~~10. Impact of the number of years used in capturing the buoyancy forced signal in CTRL.** a) box-plot of the correlation between ~~leading PC~~PC1-WB CTRL experiment and the ~~leading PC~~PC1-WB WIND experiment for different ~~extension~~number of years for the time-periods. b) Same as a) but for the correlation between PC1-WB CTRL and PC1-WB BUOY. c) Same as a) but for the ~~corrrelation~~correlation between PC1-WB CTRL and AMOC filtered with periods >2 years. The anomalies have been calculated for the long-term mean and detrended over the whole period prior the PC analysis for all experiments. Red line corresponds to the median, points

875 between 1.5 and 3 times the Inter-Quartile Range (IQR) ~~is~~are marked with crosses ~~and~~ and points outside 3 times IQR with circles. Y-axis corresponds to correlation between PCs, x-axis corresponds to number of years in all sub-periods considered. The signal extracted by 1PC-WB CTRL is always a mix of forcings however, high probability of extract buoyancy-forced signals when periods are longer than ~26 years. If period ~~are~~is longer than 35 years, the wind-forced signal is negligible.
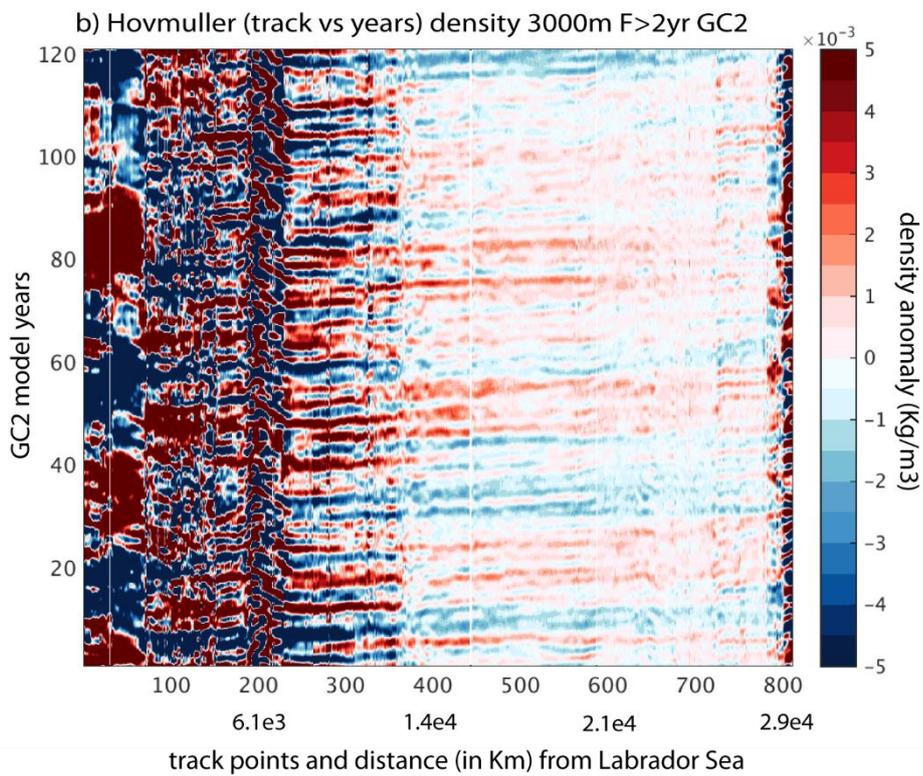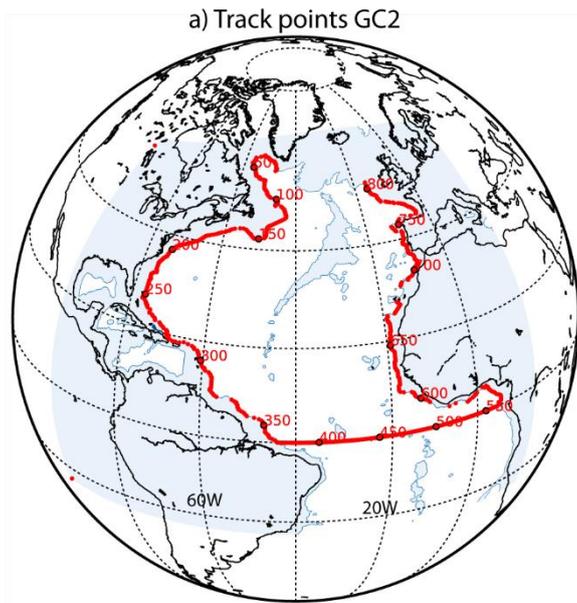
a) Track points GC2

b) Hovmuller (track vs years) density 3000m F>2yr GC2

track points and distance (in Km) from Labrador Sea

Figure ~~10~~11. Hovmöller diagram of density along the wave track in the GC2 experiment. a) The track-points correspond to the first point before the coast following the bathymetry at 3138 m in GC2. b) Hovmöller diagram of density anomalies at 3000m along the wave track, after filtering the density timeseries retaining >2 years. X-axis corresponds to track points in Fig. ~~10a~~11a and y-axis corresponds to model year.
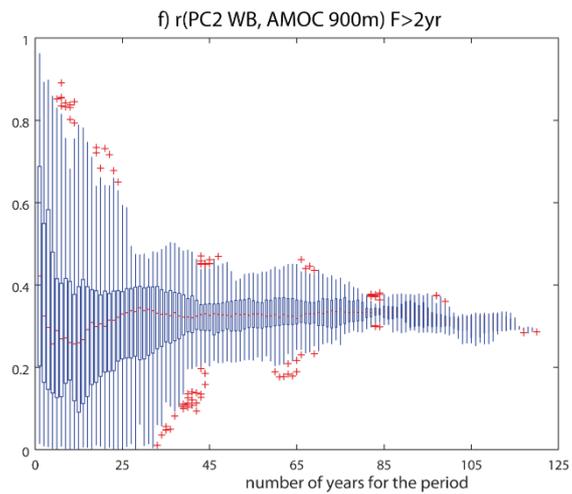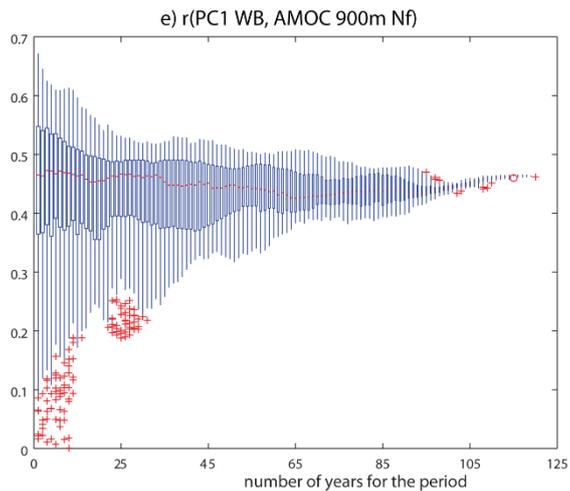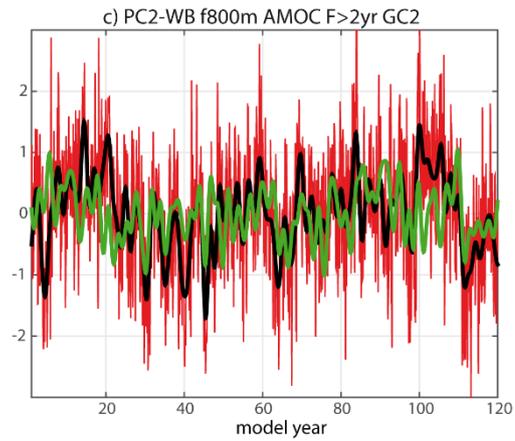
885

a) EOFs WB f800m GC2 Nf

PC1 fvar=43.8% r(PC1-AMOC)Nf=0.45
PC2 fvar=32.8% r(PC2-AMOC)Nf=0.13

b) PC1 WB f800m AMOC F>2yr GC2

PC1-Nf
PC1 F>2yr
AMOC F>2yr
r(PC1-AMOC)F>2yr=0.25

PC2-Nf
PC2 F>2yr
AMOC F>2yr
r(PC2-AMOC)F>2yr=0.32

d) Corre(AMOC, PCs-WB f800m) GC2

AMOC-PC1
AMOC-PC2

lags (months)

c) PC2-WB f800m AMOC F>2yr GC2

model year

e) r(PC1 WB, AMOC 900m Nf)

number of years for the period

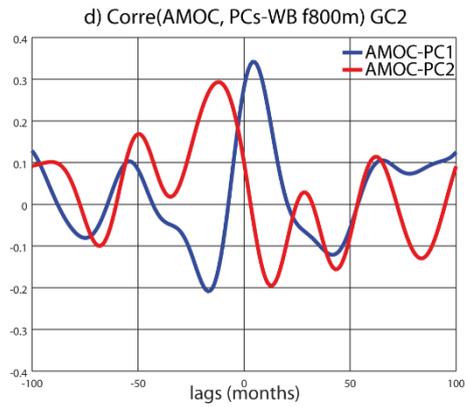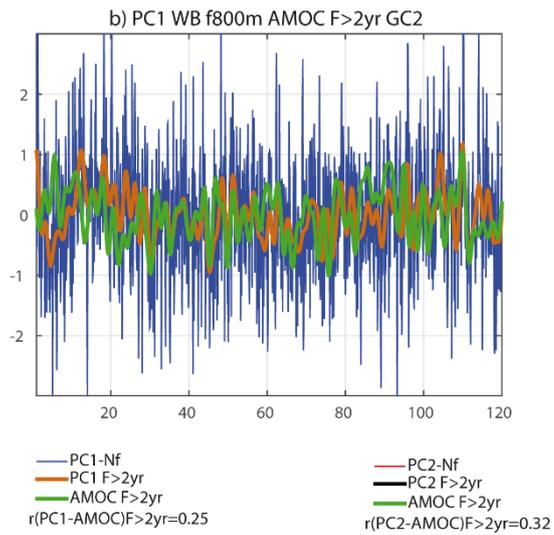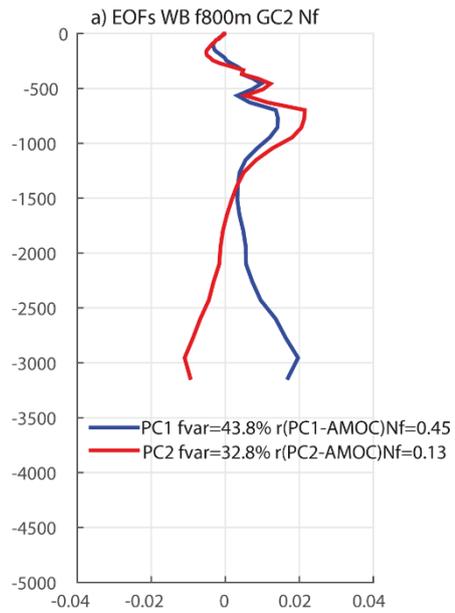f) r(PC2 WB, AMOC 900m) F>2yr

number of years for the period

Figure ~~11~~12. EOFs of WB density profiles at 26N in the GC2 experiment. a) Leading (blue line) and second (red line) EOF from WB at 26N and 76.75W in the GC2 experiment. Percentage of explained variance and correlation with the geostrophic AMOC timeseries defined at 26N and 925m depth are displayed. b) Timeseries associated with leading EOF-WB (PC1-WB, blue line), PC1-WB filtered timeseries (PC1-F>2y, brown line) and the AMOC filtered timeseries (AMOC-F>2y, green line). c) Same as b) but for the PC2-WB. d) Correlation between AMOC (at lag 0) and the first two PCs-WB (lagged). e) Correlation between PC1-WB and AMOC-Ek at 900m and 26N. Box-plot similar than Fig. ~~9c~~10c, x-axis represents number of years used in the periods for the correlation, y-axis represents correlation score. f) Same as e) but for the correlation between PC2-WB and AMOC-Ek at 900m and 26 and filtered with periodicity > 2 years.